Signals Secreted by Infection Induce Transcriptional and Epigenetic Changes in Neurons

Ellen Tedford[1τ], Norhidayah Binti Badya[1τ], Conor Laing[1], Nozomi Asaoka[2], Shuji Kaneko[2], Beatrice Maria Filippi[3], and Glenn Alan McConkey[1]*

[1] School of Biology, Faculty of Biological Sciences, University of Leeds, Leeds, UK

[2]Department of Molecular Pharmacology, Graduate School of Pharmaceutical Sciences, Kyoto University, 46-29 Yoshida-Shimoadachi-cho, Sakyo-ku, Kyoto, 606-8501, Japan

[3]School of Biomedical Sciences, Faculty of Biological Sciences, University of Leeds, Leeds, UK

*G.A.McConkey@Leeds.ac.uk
School of Biology, University of Leeds, Leeds LS2 9JT, United Kingdom

Current affiliation: E.T., University of Cambridge, UK; N.B.B., Universiti Sultan Zainal Abidin, Malaysia

Short title: Induced inter-neuronal signalling

ABSTRACT

Infection with the protozoan *Toxoplasma gondii* induces changes in neurotransmission, neuroinflammation, and behavior. Yet, it remains elusive how these changes are wrought by the small percentage of neurons that are infected. In this study we investigated how neurotransmission is altered in uninfected neurons during infection by studying suppression of noradrenergic signalling. Noradrenergic signalling is central in modulating the neuroinflammatory response. Previous studies found decreased norepinephrine and down-regulation of the synthetic enzyme dopamine ß-hydroxylase (*DBH*) during chronic infection. Here, extracellular vesicles (ie. exosomes) were isolated from infected cultures that induced transcriptional gene silencing of *DBH* and DNA hypermethylation upstream of the DBH gene. Intracerebral injection of these extracellular vesicles induced *DBH* down-regulation in the *locus coeruleus* region of the brain and contained an antisense lncRNA. Thus, global changes invoked by signals released from infected neural cells may help explain the parasite-induced behavior

changes. This novel form of paracrine signalling may apply to other neurotropic infections and enhance our understanding of regulation of neurologic functions.

INTRODUCTION

Host-pathogen interactions are a delicate balance between host mortality and elimination of the pathogen by host responses before transmission to another host. *Toxoplasma gondii*, an intracellular protozoan in the genus with the malaria parasite *Plasmodium* and one of the most successful parasites, achieves this balance during latent stages of infection. This zoonotic pathogen, that infects warm-blood animals and is able to infect humans, establishes chronic infection encysted in brain and muscle tissue. During this period, alterations in the host maintain the chronic infection and increase transmission. *T. gondii* manipulates the host at the cellular and organismal level. Following a vigorous immune response to initial infection, inflammatory responses maintain slow-growing bradyzoite stages and suppress active tachyzoite reproduction. The host exerts long lasting immune responses in the brain during chronic infection (*1–3*). *T. gondii* infection also alters behavior of the host, at least in rodents, that favors transmission to the definitive feline host. (*4–6*). The changes are associated with neurotransmitter modifications and neuroinflammation although the mechanisms responsible are poorly understood (*7–13*). Seropositivity in humans ranges from 10-90% in different parts of the world with >40m people in the USA carrying the parasite (DPDx, Centers for Disease Control, USA). *T. gondii* seroprevalence and serointensity has been correlated with neurological disorders including depression, ADHD, epileptic seizures, movement disorders, and, repeated in numerous studies, schizophrenia (*2*, *14–17*). Increased risk-taking and behavior deficits in learning and memory have also been associated with *T. gondii* infection in animal models and human subjects (*18–20*).

In recent studies, we and others described a major decrease in norepinephrine (NE) concentrations in brains from infected rodents (*9*, *13*). The enzyme responsible for NE synthesis, dopamine ß-hydroxylase (*DBH*), was down-regulated 32 ± 2.1-fold relative to uninfected animals (p= 0.0023) in rats. Central nervous system NE is involved in fear, alertness, depression, movement, socialness, anxiety, and memory. Levels of NE in the brain directly correlate with noradrenergic-linked behaviours (including locomotion, sociability, and anxiety) and this correlation was similarly found with *T. gondii* infection (*9*, *13*, *21*, *22*). Decreased NE in the CNS is likely to enhance neuroinflammation as NE also suppresses inflammatory cytokines (*23*, *24*). Indeed, the decrease in NE would be expected to exacerbate the neuroinflammatory response from astrocytes and microglia (*25*). This complex host-pathogen interaction also affects other neuronal signalling pathways with changes in GABA, glutamate, dopamine, and serotonin (*10*, *11*, *26*, *27*). The observed elevated dopamine and its metabolites found in some studies whilst not in others may be a result of the down-regulation of DBH since that decreases dopamine metabolism as well as differences in methods and strains. Remarkably, the *DBH* down-regulation was also observed *in vitro* in *T. gondii* infected catecholaminergic cells in the absence of an immune response (*13*). *DBH* was the most significantly altered gene in a transcriptome analysis and the down-regulation was observed in both rat catecholaminergic and human neuronal cells. In contrast, *DBH* expression was unchanged in cells infected with cytomegalovirus (CMV). The study here investigates the mechanism responsible for the massive down-regulation in DBH during *T. gondii* infection.

Hundreds to thousands of cysts, which reside exclusively in neurons in the brain, are found in infected rodents yet this represents only a small percentage of the $>10^8$ neurons in a rat brain. Only 0.002-0.14% of the neurons contained tissue cysts of the eleven parasite strains tested in the largest study to date of *T. gondii* in rat brains (*28*). The infected neurons were widely distributed through the brain. How this low percentage of infected neurons, that appear

primarily stoichiometrically located with only weak bias towards the amygdala, can exhibit global changes in the neurons and neurotransmitters is unknown (*6*). Further, the means by which a minor number of altered neurons in different brain areas exert consistent behavior changes between individuals is unexplained. This makes it difficult to interpret the previously observed NE and DBH down-regulation *in vitro* and *in vivo*. Hence, in this study, we explored this conundrum; identifying a novel signalling mechanism by which infected cells induce transcriptional silencing and epigenetic changes in uninfected neurons. This may have implications for neurotransmitter regulation and cognitive processes beyond parasitology.

RESULTS

Transcriptional Gene Silencing of DBH and Upstream Epigenetic Changes with Infection

Global levels of NE and the enzyme responsible for its synthesis, DBH, were decreased in *T. gondii*-infected rat brains with a direct correlation between the two (Fig. S1) (*13*). This correlation was also observed *in vitro* with decreased concentrations of DBH mRNA and NE in infected rat and human (catecholamine-producing) dopaminergic/noradrenergic cells (termed noradrenergic cells through the text). The mechanism responsible for this suppression in NE production was examined to determine whether the down-regulation was at the transcriptional or post-transcriptional levels. A nuclear run-on assay was developed to measure *de novo* transcription nuclei isolated from infected cell cultures. Nascent RNA was measured by immunocapture of biotin-UTP incorporated during transcription assays of isolated nuclei. Lower amounts of nascent *DBH* mRNA (relative to standards) was found in host cell nuclei from infected than uninfected cultures of rat noradrenergic cells (21±1.6-fold, p= 0.00062) (Fig. 1A). Similarly, *de novo* transcription of *DBH* was downregulated in human neuronal

noradrenergic cells (21±1.7-fold, p= 0.032) (Fig. 1B). Hence, *DBH* down-regulation in human and rat noradrenergic cells is due to transcriptional gene silencing (TGS).

As *DBH* expression was down-regulated at the transcriptional level, the epigenetic state of the *DBH* gene was investigated (*29*). Methylation Sensitive Restriction Enzyme qPCR (MSRE-qPCR) was used to monitor DNA methylation levels in the *DBH* upstream region where the majority of CpGs are clustered (Fig. 1C). Methylation in the *DBH* upstream region rose from 16±4.6% to 66±3.8% in infected cultures of rat noradrenergic cells during the course of the infection (Fig. 1D; p=0.00072). As the neuronal cells (ie. neurotransmitter synthesis, synaptic transmission) are sensitive to pH changes (*30*, *31*), alkaline-shocked tachyzoites (as previously described) were used for *in vitro* infections (*32*). This procedure enhances bradyzoite conversion and elevated expression of bradyzoite markers BAG1 and SAG4 (E. Tedford PhD thesis). Infected human neuronal cultures also exhibited *DBH* hypermethylation with a time-dependent increase; greater than double (2.8-fold; range 2.3-4.8-fold) the methylation in uninfected cells (Fig. 1E; p=0.0011).

To examine the effects of *T. gondii* on *DBH* in neurons, *ex-vivo* infection of prefrontal cortex, nucleus accumbens and ventral tegmental area brain slices was examined (*33*). Methylation of the *DBH* upstream region rose from 29±2.7% in the organotypic brain tissue slices to 74±4.6% in the most infected slices (p= 0.000051) (Fig. 2A). Next, the DNA methylation levels were analysed in the brains of chronically-infected mice. Neurons were purified by FACS and the *DBH* methylation was measured. The infected animals had 53±7.7% methylation of *DBH* compared to 6.3±2.0% in uninfected mice (p= 0.000045, Fig. 2B). This eight-fold higher level of *DBH* methylation in the brains of infected animals is not the result of general changes in DNA methylation as global genomic methylation levels were unchanged in neurons and cell lines with infection (Fig. 2C). Hypermethylation of CpG residues upstream of the *DBH* gene were also found in NGS genomic bisulfite sequencing of infected cultures (Fig. SF2).

The roles for DNA methyltransferase (DNMT) and histone deacetylation in the process of the TGS and the epigenetic changes were investigated. Infected noradrenergic cells were treated with the DNMT inhibitors RG108 and 5-azacytidine (5-AC). Both compounds disrupted the *DBH* down-regulation and DNA hypermethylation in the rat noradrenergic cells (Figs. 3A, 3C). The DNMT inhibitors also blocked the parasite-induced *DBH* down-regulation and DNA hypermethylation in human neuronal cells (Figs. 3B, 3D). This was not due to parasite sensitivity to the inhibitors since *T. gondii* lacks 5-methylcytosine and the inhibitors were non-toxic to parasites at concentrations tested (data not shown) (*34*). The histone deacetylase inhibitor trichostatin A did not abrogate the *DBH* down-regulation or hypermethylation in infected cultures (Fig. 3). Hence, the *DBH* silencing involves DNMT but may differ from mechanisms involving histone deacetylation.

Infected Neuronal Cells Secrete a Signalling Factor

We noted that changes in *DBH* and NE concentrations in the infected animals were readily measurable even though the majority of neurons are not infected. Indeed, tissue cysts are only found in a very low percentage of the neurons (*28*). This suggested to us that uninfected neurons were also affected. Hence, we investigated the possibility that transcriptional changes are induced in uninfected neurons by a transmissible signal from infected cells. Transmission of the epigenetic changes to exposed, uninfected neuronal cells was examined by comparing cell populations enriched for GFP-expressing *T. gondii* (GFP+) cells and uninfected (GFP-) cells in the same culture (Fig. 4A, 4B). *DBH* hypermethylation was found in both the infected and uninfected populations of cells in the parasitized culture (Fig. 4B; ANOVA test, $p= 0.0089$). Indeed, the uninfected cells had DNA methylation levels at least equal to the GFP+ cells.

To delineate how transcriptional and epigenetic alterations were induced in the uninfected cells, we first investigated whether contact with parasites or infected cells is required for the

alterations. A transwell system was used that permits uninfected cells to be exposed to *T. gondii*-infected cell products. This set up was used because it differentiates between diffusible signals and parasites injecting components into cells without invasion, as was observed with a Cre/*loxP* assay in infected mouse brains (*35*). *DBH* expression in uninfected rat noradrenergic cells in the bottom reservoir of the transwell system with the top reservoir containing an infected culture was measured (Fig. 4C). *DBH* expression in the cells exposed to infected cultures was found to be down-regulated 7.9±2.8-fold (Fig. 4D) suggesting that a transmissible factor was released from infected cells. In contrast, noradrenergic cells that were exposed to cultures containing heat-killed *T. gondii* ('mock-infected') were unchanged in *DBH* expression (Fig. 4D). Exposure of a human neuronal cell line to infected cells induced an even more striking decrease in *DBH* expression (37±16-fold, p=0.0038) (Fig. 4E). The separation of parasites into the upper and lower reservoirs by the 0.4 μm filter was confirmed by inoculating HFF cells with media removed from both reservoirs (data not shown). Further, infected HFF cultures in the transwell system did not induce *DBH* down-regulation in exposed (uninfected) noradrenergic cells (Fig. 4F).

Using the transwell system, the methylation of the *DBH* upstream region in exposed, uninfected noradrenergic cells was examined. *DBH* upstream methylation was measured by MSRE qPCR in PC12 cells exposed to *T. gondii*-infected cells. Methylation of the *DBH* 5' region was 44±5.5% higher (p=0.0013) in cells exposed to infected cells compared to exposure to uninfected cultures (Figure 4G). We also examined human neuronal M17 cells and found that exposure to permeable factors from infected cells induced an increase of 49±19% (p=0.0003) methylation of the DBH upstream region (Figure 4H). Hence, *T. gondii*-infected noradrenergic cells release a permeable signalling factor that elicits down-regulation of *DBH* gene expression and hypermethylation of the upstream region in rat and human noradrenergic cells.

Extracellular Vesicles Transmit Gene Silencing to Uninfected Neurons

The permeable effector that down-regulates *DBH* may be a soluble factor such as an immune molecule or a packaged signal. Insoluble components separated from soluble factors by ultracentrifugation tested positive in preliminary tests for *DBH* down-regulating activity (data not shown). Many cells of the CNS can release extracellular vesicles (EVs) including astrocytes, glia, oligodendrocytes, Schwann cells and neurons (*36–38*). EV secretion is emerging as an important mechanism of cellular communication within the CNS (*39*). Initially, we tested the potential involvement of EVs by treating cells with an inhibitor of EV biogenesis whilst being exposed to infected cultures. The cells were examined for the effect on the *DBH* hypermethylation phenotype. Treatment of rat noradrenergic cells in the transwell system with GW4869, that inhibits sphingomyelinase required for vesicle budding in endosomal formation, abrogated the *DBH* hypermethylation in cells exposed to infected cultures (Fig. 5A). This suggested that EVs might be involved in the TGS and epigenetic changes in *DBH*.

EVs were purified from infected cultures by ultracentrifugation and sucrose-gradients (*40*, *41*) (Fig. 5B). The purified vesicles were exhaustively characterized for size, morphology, sedimentation rate, canonical exosome markers, and filtration following MISEV2018 guidelines (*42*). The 68-71 nm size of the EVs (fitting the terminology 'exosomes') and their abundance did not differ ($p > 0.05$) between EVs isolated from infected and control cultures (Figs. 5C, 5D, Fig. SF3). When noradrenergic cells were treated with purified EVs, only those from infected cultures induced *DBH* down-regulation (190±67-fold, $p=0.006$ in Fig. 5E).

The EVs from infected cells, iEVs, were tested for their ability to induce epigenetic changes in uninfected cells. *DBH* hypermethylation was examined using the MSRE-qPCR assay as described above. Methylation increased from 16±3.9% to 81±7.9% over the course of the experiment. In a time course of exposure to the infected culture, methylation was unchanged

after 24 or 48 hours of exposure but hypermethylation was observed at 96 hours of incubation (Fig. 5F; Anova p=0.00080).

The effect of the iEVs on neurons in rats was examined. Sucrose-gradient purified EVs from infected noradrenergic cells were injected by intracranial injection into the *locus coeruleus* (LC) of adult rats and *DBH* expression was measured (Fig. 6A, Fig. SF4). The LC is the central region of noradrenergic cells in the brain. Injection of iEVs induced a decrease in *DBH* mRNA (62±43-fold, p=0.0079) in neurons in the hindbrain, which includes the LC (Fig. 6B) compared to treating with EVs from uninfected cultures (relative to the neuronal marker *MAP2*). *DBH* mRNA levels in the mid-brain and prefrontal cortex did not differ in rats receiving the iEVs. In these experiments, the health parameters (body weight, appearance and food intake) were normal in treated rats and expression of an independent gene was not altered between the treatments in the brain samples (Fig. SF5). Further, *DBH* expression in the adrenal glands was unaffected by the treatments (data not shown). The decrease in *DBH* mRNA observed with intracranial EV injection was similar to that observed in chronic infections and hence can explain the observed change in noradrenergic-linked behaviours (*13*).

EVs from Infected Cells Contain an Antisense *DBH* lncRNA

We investigated the mechanism by which the iEVs induce the epigenetic silencing. Initially, the sensitivity of the EVs to RNA-degrading ultraviolet (UV) radiation was tested to assess the potential involvement of an RNA component (*43*). The iEVs treated with UV radiation no longer induced hypermethylation of the *DBH* promoter (Fig. S11). Proteomic analysis of the iEV contents by LC-MS/MS did not identify any proteins involved in *DBH* expression (data not shown).

Non-coding RNAs (ncRNA) are involved in regulating gene expression with roles in neuronal gene expression with long non-coding RNA (lncRNA) such as antisense transcripts providing

high specificity (*44–46*). EVs have been found to contain miRNAs and lncRNAs, although their functional significance is still unclear. With the specificity of the *DBH* down-regulation in *T. gondii*-infected noradrenergic cells and the magnitude with iEV treatment, a search for an antisense long non-coding RNA (lncRNA) was performed (*44*, *47*). A panel of primers walking upstream stepwise from the *DBH* coding region were used to screen for an antisense RNA (*29*). These identified a lncRNA in infected cultures (Fig. SF7). EVs purified from infected cells were then tested and found to contain the *DBH* antisense lncRNA (Fig. 6C, 6D, Fig. SF8). The lncRNA is complementary to the *DBH* upstream region containing cis-regulatory elements and crosses the transcription start site. As a positive control for samples, miR-21 miRNA served to confirm RNA quality purified from the EVs (*48*). Intriguingly, the timeframe observed for the *DBH* hypermethylation (Fig. 5F) is similar to dynamic DNA methylation changes observed in human cells treated with promoter targeted antisense RNA (*49*). The observations above represent the first study to show a specific and functionally-relevant lncRNA to be transmitted from one neuronal cell to another (*50*).

Recently, a consensus sequence for chromatin-bound lncRNAs was identified (*51*). The sequence was found to be the recognition site for U1 snRNP that is complementary to the 9-nucleotide 5′ targeting sequence of U1 snRNA. The U1 snRNP was important for lncRNA to bind the chromatin and interacts with bound RNA polymerase II. The *DBH* antisense lncRNA was found to contain the conserved U1 snRNP recognition site. Further, predicted secondary structure analysis places the U1 snRNP recognition site in a loop region in minimum free energy secondary structures of *DBH* antisense lncRNA (Fig. 6F). It is important for the U1 recognition site to be in a loop region to permit binding of the lncRNA to U1 snRNA. Future experiments will further investigate this novel induced lncRNA.

DISCUSSION

Infection of neuronal cells by *T. gondii* resulted in epigenetic silencing of *DBH* with transcriptional down-regulation and DNA hypermethylation upstream of the gene both within infected cells and transmitted to neighbouring cells by extracellular vesicles. The data provide an explanation for how infection of a limited number of neurons imposes widespread host gene regulation. As shown in numerous publications since the 1970's, reduced CNS noradrenergic signalling via decreased NE synthesis causes noradrenergic-linked behaviour changes and, hence, the widespread *DBH* down-regulation provides an explanation for changes in noradrenergic-linked behaviours in chronically-infected mice (*13*, *52*). We propose a model of *T. gondii* inducing host-encoded lncRNAs that are packaged and released from host neuronal cells during chronic infection to modulate the host environment; extending studies that found *T. gondii*-infected fibroblasts and macrophages can induce host lncRNAs (*53*). In this study, iEVs spread to uninfected neurons regulating gene expression and modifying chromatin in target cells. This mechanism may affect expression of other host genes and could explain earlier observations of hypomethylation of a host arginine vasopressin promoter in the amygdala of *T. gondii*-infected animals (*54*). The *DBH* antisense lncRNA contains a chromatin localization signal and hence may silence expression of *DBH* via U1 snRNP binding at the transcriptionally active *DBH* gene and interacting with RNA polymerase II. This would disrupt transcription and permit DNA methylation. In this study, products of infected fibroblasts did not induce the *DBH* down-regulation (Fig. S2). In the future it will be interesting to assess the intercellular crosstalk from infected neurons to different brain cell types and to examine how *T. gondii* induces host cells to express and package selective lncRNAs.

The findings in this study describe a novel form of regulating neurotransmission that may contribute to the balance for maintaining chronic infection. Prior studies have found that EVs can contain proteins that regulate neurogenesis and neuronal connectivity (*43*). Whereas this

study described an lncRNA packaged into EVs that specifically altered neurotransmitter signalling. This mechanism unifies observed decreased norepinephrine in the brains of chronically-infected rodents and resultant behavior changes. Reduced DBH also elevates dopamine release from LC neurons such as those modulating learning and memory (*9*, *55*) and may explain the increased dopamine signalling (*56*). As NE modulates the cerebral immune response via adrenergic receptors on astrocytes and microglia, changes in NE levels will affect neuroinflammatory responses that are crucial in maintaining the balance of latent, long-lasting infection (*23*, *24*). Neuroinflammation changes may also explain anxiety and increased risk-taking in *T. gondii* infected mice, particularly the observed restoration of normal behaviour in infected mice treated with a noradrenergic agonist (*2*, *57*). Finding that EVs can modify DNA methylation of neurons may further represent a mechanism beyond parasitic machinery, in innate neurophysiological function, and enhance our understanding of the role of dynamic DNA methylation in memory and learning.

METHODS

Cell culture

Parasite and Cell Culturing

T. gondii Prugniaud strain, isolated from mouse neuronal cysts, was used unless otherwise stated. Parasites were maintained in monolayer cultures of human foreskin fibroblasts (HFFs, ATCC® SCRC-1041) in Dulbecco's Modified Eagles Medium (DMEM, GIBCO, USA) containing 10% foetal bovine serum (FBS) and 20 $\mu g/ml^{-1}$ penicillin/streptmycin (Sigma, USA). Incubation of free tachyzoites in pH 8.2 DMEM with 5% FBS, overnight at 37°C was used to induce tachyzoites conversion to bradyzoites as previously described (*13*). Expression of *T. gondii* differentiation markers over 5 days of infection confirmed bradyzoite conversion

(data not shown). All experiments were performed with induced parasites unless otherwise stated.

Rat adrenal phaeochromocytoma, PC12, (ATCC® CRL-1721) cells were maintained at a density of 2-8x10^5 cells/ml in Roswell Park Memorial Institute (RPMI) 1640 Medium (GIBCO, USA) and supplemented with 10% horse serum (GIBCO, USA), 5% FBS (GIBCO, USA) and 20 μg/ml^{-1} penicillin streptomycin (Sigma, USA). Human neuronal BE(2)- M17 cells (ATCC® CRL-2267) were maintained in a 1:1 ratio of F12 Hams and OptiMEM (GIBCO, USA) media supplemented with 10% horse serum (GIBCO, USA), 5% FBS (GIBCO, USA) and 20 μg/ml^{-1} penicillin streptomycin (Sigma, USA). The production of dopamine (DA) and norepinephrine (NE) by these cell lines was monitored regularly by HPLC-electrochemical detection. For experiments in which Extracellular vesicles (EV) were harvested or analysed, exosome free-FBS (GIBCO, USA) replaced the serum in the media for 24 hours prior to harvest. All cells were maintained at 5% carbon dioxide and 37°C and monitored for growth by light microscopy.

Infection of PC12 and BE(2)- M17 cells

Cells were cultured in multi-well plates at a density of 5x10^4 cells/ml. When stated, transwell plates (Nunc™ cell culture inserts, Thermo Scientific) were used, with cells plated at 2.5 x 10^4 cells/ml. Following 24 h of growth on 6-well plates, cells were infected with induced Prugniaud parasites in upper-wells, maintaining a multiplicity of infection (MOI) of 1. Cells were harvested immediately following infection (day 0) and after 3 and 5 days of infection for downstream processing. Mock-infection was performed using heat-killed *T. gondii* parasites subjected to 80°C for 10 minutes. The cultures were monitored daily by light microscopy.

Treatment of cells with purified extracellular vesicles

EVs were extracted and purified from cell medium as described below. PC12 cells were plated on 6-well plates and grown to a density of $2x10^4$ cells/ml. Cultures were treated with EVs at a 10:1 culture media concentration equivalent (ie. 1 ml of PC12 cell culture treated with EVs purified from 10 ml of culture). Cells were treated every 24 h. DNA and RNA were harvested 24 h after the last treatment.

Drug assays

Cells were cultured and infected as previously described. Drug was added one hour before the time of infection (day 0). Cultures were grown in media containing a range of inhibitor concentrations; GW4869 (0-100 nM), Trichostatin A (TSA, 0-100 nM), RG108 (0-100 nM), or 5-Azacytidine (5-AC, 0-50µM) (SIGMA, USA). The effect of drug treatment on the parasites was monitored by infecting human fibroblasts with KU80-GFP bradyzoites or RH-YFP tachyzoites (*58*, *59*) growth was measured by fluorescence using a FLUOstar Omega plate reader (BMG, UK).

Fluorescence-assisted cell sorting (FACS) of infected human neuronal cells

Human neuronal cells were infected with the Pru Δhpt/GFP/FLUC *T. gondii* strain, (kind gift from Boothroyd) (*60*). Five day infected and uninfected cell cultures were resuspended in PBS and separated in a CytoFLEX–2 flow cytometer (Becton Dickenson, USA) to isolate negative and GFP+ fluorescent cells. Control uninfected cell cultures were also subjected to FACS. DNA was extracted and purified from FACS populations.

Animal Work

Organotypic brain slice cultures

All animal care and experimental procedures were approved by the Kyoto University Animal Research Committee. These experiments were performed with the help and guidance of the Kaneko Laboratory at Kyoto University. Sectioning was performed as described (*33*). Sprague-Dawley rat pups at postnatal days 3-4 were anesthetized by hypothermia. Brain was removed and separated into two hemispheres. Coronal sections (350µm thickness) were prepared under sterile conditions. Slices were dissected to include the ventral tegmental area (VTA). These slice cultures were placed on 30 mm insert membranes (Millicell 0.4µm; Millipore). Slice culture medium contained RPMI supplemented with 10% horse serum (GIBCO, USA), 5% FBS and additional 6.5 mg/ml glucose and 2 mM l-glutamine. The brain slice cultures were cultured at 37°C in a 5% CO^2 for 15 days after dissection prior to use in experiments.

Rodent Infections

Brain samples were supplied from animal experiments conducted at the University of Leeds research animal facility with procedures approved by the University Animal Care and Use Committee and following Home Office, HSE, regulations and guidelines for Animals (Scientific Procedures) Act 1986 published in 2014 and with considerations of the replacement, reduction, and refinement in the use of animals for research.

Mice

Mice were housed up to five to a cage and maintained on a standard light-dark cycle with access to chow diet and water *ad libitum*. Throughout the experiments animals were monitored for illness or weight loss (more than 25%) and sacrificed 5-6 weeks after infection. Mice used were BALB/cAnNCrl x C57BL/6NCrl) F1 generation male mice. The mouse infections, brain dissection and frozen cryostat sectioning was performed as described (*13*).

Rats

All rat experiments were undertaken as previously described (*13*) prior to tissue sampling. Male Lister Hood rats (Harlan Ltd, UK) were used for all experiments. Rats were housed in individual cages and maintained on a standard light-dark cycle with access to chow diet and water *ad libitum*. Animals were infected by intraperitoneal (IP) injection with tachyzoites. Throughout the experiments animals were monitored for illness or weight loss (more than 25%) and sacrificed 5-6 months post-infection. Brains were snap-frozen for cryosectioning and RNA extraction.

Extracellular vesicle intracerebral treatment

Intracerebral injection into adult rats followed previously described experimental procedures (*61*). EVs were extracted and purified from rat catecholaminergic PC12 cells as described below. Eight-week-old male Sprague-Dawley rats weighing between 260 and 280g (Charles River Laboratories) were used. Rats were housed in individual cages and maintained on a standard light-dark cycle with access to chow diet and water *ad libitum*. Rats were stereotactically (David Kopf Instruments) implanted with indwelling bilateral cannula targeting the locus coeruleus. Health status was monitored visually and by food consumption (appetite) and body weight. After one week of recovery, implanted rats received a 2 µl infusion twice a day for 3 days with purified EVs (4 µg protein) isolated from infected or uninfected PC12 cells. On the fourth day rats were anaesthetized and received an injection 3 µl bromophenol blue through each side of the bilateral DVC cannula (to verify their placement) prior to harvesting brain tissue. Brain tissue was dissected into prefrontal cortex, midbrain, and hindbrain regions for processing for RNA.

Fluorescence-assisted cell sorting (FACS) of mouse neurons

Mouse brain samples were processed as described (*62*). Briefly, brains were suspended in lysis buffer (0.32M sucrose; 0.1mM ethylenediaminetetraacetic acid; 5mM $CaCl_2$; 3mM $Mg(Acetate)_2$; 10mM Tris-HCl pH 8; 1mM dithiothreitol; and 0.1% Triton X-100) and processed using a 15 ml glass dounce homogenizer (Wheaton, UK) in 5-10 strokes on ice. Samples were centrifuged at 100,000xg with a two-step sucrose gradient to purify nuclei. Nuclei were stained with primary antibody NeuN (Abcam, EPR12763 1:250) and secondary antibody Alexa-488 (Abcam, ab150077, 1:1000). All nuclei were also stained with Hoechst 33342 (SIGMA, USA). Samples were sorted using the Becton Dickinson FACSAria II system.

Extracellular vesicle characterization

Extracellular vesicle purification

EVs were isolated from media by ultracentrifugation as described (*63*, *64*). Briefly, one day prior to harvest, complete media was replaced with media containing exosome-free FBS (System Bioscience, CA). Cell cultures of uninfected and infected cells (five days following infection) were harvested and centrifuged at 3000xg for 10 minutes at 4°C. The supernatant was isolated and centrifuged at 160,000xg for 2 hours in a Type 60 Ti fixed angle rotor at 4°C. The pellet was resuspended in one ml of 90% sucrose. Eleven layers of one ml of sucrose 70%-10% w/v were then added and centrifuged at 70,000xg for 16 hours at 4°C in a Type 60 Ti fixed angle rotor. Supernatant was collected in two ml fractions. PBS (8 ml) was added to the fraction with a density corresponding to that of EVs and centrifuged at 160,000xg for 70 minutes at 4°C to recover purified EVs.

UV Ablation

Purified EVs were isolated as described. Prior to UV treatment, DBH down-regulation was verified for 24 hour treated cells. EVs were exposed or mock exposed to UV light at 290nm for 5 minutes at 4°C.

Western blotting

Western blotting was performed using the Exo-Check Exosome Antibody Array (Systems Bioscience, CA) as per manufacturer's instructions. Briefly, 500 µg protein equivalent of purified EVs isolated from PC12 culture were lysed and ligated to horseradish peroxidase (HRP) overnight at 4°C. Ligated protein was then incubated with the antibody membrane for two hours at room temperature. After three washes SuperSignal West Femto Chemiluminescent Substrate kit (Thermo Scientific, UK) was used as per manufacturer's instructions. The blot was visualised via 90 second exposure to X ray film. Film was developed using the Konica SRX-101A Tabletop Processor.

Transmission electron microscopy (TEM)

EVs were purified as described above. Electron microscopy was performed as described (*65*). Freshly isolated EVs were resuspended in cold Dulbecco Phosphate-Buffered Saline (DPBS) containing 2% paraformaldehyde. Exosomes were mounted on copper grids, fixed with 1% glutaraldehyde in cold DPBS for 5 minutes at room temperature, negative stain was performed with uranyl-oxalate solution at pH 7 for 5 min, and embedded with methyl cellulose-UA for 10 min at 4°C. Excess cellulose was removed, and samples were dried for permanent preservation. Electron microscopy was performed in the University of Leeds facility using a Titan Krios 2 electron microscope. Analysis and extracellular vesicle diameter were measured using ImageJ software.

Molecular Techniques

DNA Extraction

Classic phenol-chloroform method extraction was performed as described in (*66*). Briefly, tissue samples were first homogenised using a Micro Tissue Homogenizer (Fisher Scientific, UK). Homogenised tissue or cell pellets were incubated at 56°C overnight with 20 mg/ml Proteinase K. An equal amount of phenol/chloroform/isoamyl alcohol (PCI) solution (25:24:1) was then added, mixed and centrifuged. The aqueous layer was isolated and an equal volume of chloroform:isoamyl (CI) alcohol (24:1) added. DNA was precipitated using absolute ethanol and DNA, then resuspended in deionised water.

RNA extraction was performed using Direct-zol (Zymo, USA) as per manufacturer's instructions.

PCR

Polymerase chain reaction was performed using the GoTaq PCR master mix (Promega, USA) as per manufacturer's instructions. Samples were amplified in a 2720 thermal cycler (Applied Biosystems, USA). The PCR parameters were 94°C for 30 seconds; 35 cycles of 94°C for 30 seconds (denaturing step), 55°C for 15 seconds (annealing step) and 72°C for 10 seconds (elongation step); a final elongation of 72°C for 30 seconds.

Samples were visualised on a 2% w/v agarose gel with a Trackit 1kb Plus DNA ladder run at 80V until the DNA ladder and the sample products of interest had separated adequately.

RT-qPCR

RT-qPCR was performed using SYBR green master mix (Life Technologies, USA) as per manufacturer's instructions and run using a CFX Max Real Time PCR machine (Bio-rad,

USA). Parameters were 95°C for 2min and followed by 45 cycles of 95°C for 15 seconds, (primer Tm-5) °C for 15 seconds, and 72°C for 10 seconds. Primer sequences are recorded in Table S1.1. A melt-curve was performed to check for expected products. All RT-qPCR was performed with four technical replicates which were averaged.

Nuclear run-on

Nuclear run-on was performed as described (*67*). Briefly, after five days of infection, cells were incubated with lysis buffer containing 10 mM Tris-HCl pH 7.4, 10 mM NaCl, 3 mM MgCl2, 0.5% NP-40 at 4°C isolating nuclei. Nuclei are then suspended in transcription buffer containing 20 mM Tris-HCl pH 8.3, 5 mM MgCl2, 300 mM KCl, 4 mM DTT, RNase OUT 40 Units/µl, 0.5 mM BrUTP, 1mM ATP, 1mM GTP, 1mM CTP, 1mM UTP. Samples were incubated for 45 min at 37°C prior to RNA extraction using MEGAclear Transcription Clean-Up Kit (Life Technologies) as per manufacturer's instructions. Bead-based immunoprecipitation was performed with protein G Dynabeads and IgG anti-BrdU antibody IIB5 (Santa Cruz Biotechnology, SC-32323). RNA was extracted and RT-qPCR performed as previously described.

Methylation sensitive restriction enzyme (MSRE) quantitative PCR

DNA was extracted from cell cultures and isolated as previously described. DNA concentrations were confirmed using a Nanodrop spectrophotometer. Samples were divided into reference and test samples. Test samples were digested with the high-fidelity methylation sensitive restriction enzymes (MSRE) HpaII, MaeII and SmaI (TaiI) in the Tango buffer (Thermo Fisher Scientific, USA). These MSREs were chosen based on the restriction enzymes sites present in the DBH upstream region. Reference samples were mock digested. Digestion

was performed by heating to 25°C for 30 minutes, 37° for 30 minutes and 65° for 30 minutes. RT-qPCR was then performed. Percentage methylation calculated based on the difference in Cq values between test and reference samples. Digestion was confirmed with methylated and unmethylated human DNA standards provided with the OneStep qMethyl kit (Zymo) as per manufacturer's instructions. Additionally, primers and MSRE digestion was confirmed with MSRE-PCR. qPCR was performed using SYBR®Green Real-Time PCR Master Mix (Thermo Fisher).

Directional RT-PCR for DBH lncRNA Screening

Three single-stranded forward (ie. sense) directional primers were designed to detect antisense RNA and are labelled RT-Primer 1, RT-Primer 2, and RT-Primer 3 (Extended Data Fig. 6A). The RT-designed primers are located (1) in the first exon, (2) near the transcription start site, and (3) -378 bp upstream of the DBH coding sequence. Four pairs of PCR primers were then designed to amplify products from the RT primer synthesized-template to screen for the presence of antisense lncRNA (Extended Data Fig. 6A). A list of primers used is shown, Table S1.1.

Total RNA was extracted from *T. gondii* infected-PC12 cells that were harvested on day five post-infection using the Direct-zol RNA MiniPrep Plus kit (Zymo Research, USA) according to the manufacturer's instructions. DNase I treatment was implemented as suggested by the manufacturer. In addition, to ensure that all trace amounts of DNA contamination were removed, the eluted RNA samples were treated again with DNase enzyme using TURBO DNA-free™ kit (Invitrogen, USA) according to the manufacturer's instructions as in earlier studies (*29*). The dependence of PCR products on the RNA samples was verified by parallel experiments with RNase treatment (data not shown). RNA samples were reverse transcribed

with first strand synthesis primed with RT-primer 1 to 3 with a Maxima H Minus First Strand cDNA synthesis kit (Thermo Scientific, USA) following the manufacturer's instructions. For each of the samples, there were several controls including priming the cDNA synthesis with random hexamer primer, a negative control reaction to assess the gDNA contamination in the RNA sample containing all components for RT-PCR except the Maxima H Minus enzyme mix, and no template control to assess reagent contamination. The mixtures were incubated as follows: 25°C for 10 min, 50°C for 30 min, 65°C for 20 min and then the reaction was terminated by heating at 85°C for 5 min. The reaction products served as templates for PCR with GoTaq ® G2 Hot Start Master Mix (Promega, USA), 300 nM forward primer, 300 nM reverse primer, and 2 µl template DNA. Thermal cycling was 3 min at 95°C, followed by 30 cycles of 95°C for 30 seconds, 57°C for 30 seconds, 72°C for 20 seconds and final termination at 72°C for 5 min in a thermocycler (Applied Biosystems, USA). All PCR products were resolved and visualized by 1.5% to 2% w/v agarose gel electrophoresis. For DNA sequencing, the specific band was gel-excised and gel-extracted using QIAQuick Gel Extraction Kit (Qiagen, Germany). The eluted DNA concentrations were then measured by the NanoDrop spectrophotometer (Thermo Fisher Scientific, UK). The PCR products were subcloned into a TOPO TA cloning vector (PCRTM4-TOPO–Invitrogen TA cloning kit, Thermo Fisher Scientific, UK) and transformed into XL-10 Gold ultracompetent cells (Agilent Technologies, USA). Two clones bearing inserts of each sample were sent for Sanger Sequencing to Genewiz, UK.

Global Methylation

Global methylation was measured using a colourimetric, ELISA adapted method, MethylFlash Methylated DNA 5-mC Quantification Kit (Epigentek, US) as per manufacturer's instructions.

DNA (5 ng) was used for quantification and absorbance (405nm) was read using the Molecular Devices SPECTRA MAX PLUS Plate Reader Ver. 3.05 Spectrophotometer.

Whole-genome bisulphite sequencing

Whole-genome sequencing of uninfected and *T. gondii*-infected PC12 cells was performed at the University of Leeds Next Generation Sequencing facility at St James Hospital. DNA samples were collected by phenol-chloroform extraction as previously described. Five biological replicates were pooled for uninfected and control samples. Libraries were prepared using the TruSeq DNA Methylation Kit (Illumina, UK). Briefly, samples were bisulphite treated using the EZ DNA Methylation-Gold Kit (Zymo). Treated DNA was then amplified and 5' adapters ligated. 3' indexing adapters were then ligated to the ssDNA and 12 rounds of PCR performed. Sequencing was performed using the HiSeq 4000 Systems (Illumina). Differential methylation between infected and uninfected samples was calculated based on genome alignments by the Facility.

Statistical Analysis

All statistical analysis was performed using GraphPad and SPSS. For each data set, Levene's test of equal variance was performed. Unless otherwise stated, a student t test and where appropriate ANOVA with a post hoc test were performed for all equally distributed data.

REFERENCES

1. K. J. Pittman, M. T. Aliota, L. J. Knoll, Dual transcriptional profiling of mice and Toxoplasma gondii during acute and chronic infection. *BMC Genomics*. **15**, 806–11 (2014).
2. M. Boillat, P.-M. Hammoudi, S. K. Dogga, S. Pagès, M. Goubran, I. Rodriguez, D. Soldati-Favre, Neuroinflammation-Associated Aspecific Manipulation of Mouse Predator Fear by Toxoplasma gondii. *Cell Rep.* **30**, 320-334.e6 (2020).
3. H. M. Ngô, Y. Zhou, H. Lorenzi, K. Wang, T.-K. Kim, Y. Zhou, K. El Bissati, E. Mui, L. Fraczek, S. V Rajagopala, C. W. Roberts, F. L. Henriquez, A. Montpetit, J. M. Blackwell, S. E. Jamieson, K. Wheeler, I. J. Begeman, C. Naranjo-Galvis, N. Alliey-Rodriguez, R. G. Davis, L. Soroceanu, C. Cobbs, D. A. Steindler, K. Boyer, A. G. Noble, C. N. Swisher, P. T. Heydemann, P. Rabiah, S. Withers, P. Soteropoulos, L. Hood, R. McLeod, Toxoplasma Modulates Signature Pathways of Human Epilepsy, Neurodegeneration & Cancer. *Sci. Rep.* **7**, 96–114 (2017).
4. J. P. Webster, C. F. Brunton, D. W. MacDonald, Effect of Toxoplasma gondii upon neophobic behaviour in wild brown rats, Rattus norvegicus. *Parasitology*. **109**, 37–43 (1994).
5. M. Berdoy, J. P. Webster, D. W. Macdonald, Fatal attraction in rats infected with Toxoplasma gondii. *Proc. R. Soc. B Biol. Sci.* **267**, 1591–1594 (2000).
6. A. Vyas, S.-K. Kim, N. Giacomini, J. C. Boothroyd, R. M. Sapolsky, Behavioral changes induced by Toxoplasma infection of rodents are highly specific to aversion of cat odors. *Proc. Natl. Acad. Sci. U. S. A.* **104**, 6442–6447 (2007).
7. C. Konradt, N. Ueno, D. A. Christian, J. H. Delong, G. H. Pritchard, J. Herz, D. J. Bzik, A. A. Koshy, D. B. McGavern, M. B. Lodoen, C. A. Hunter, Endothelial cells are a replicative niche for entry of Toxoplasma gondii to the central nervous system. *Nat. Microbiol.* **1**, 16001 (2016).
8. W. M. Hutchison, P. P. Aitken, B. W. P. Wells, Chronic toxoplasma infections and motor performance in the mouse. *Ann. Trop. Med. Parasitol.* **74**, 507–510 (1980).
9. F. Ihara, M. Nishimura, Y. Muroi, M. E. Mahmoud, N. Yokoyama, K. Nagamune, Y. Nishikawa, Toxoplasma gondii infection in mice impairs long-term fear memory consolidation through dysfunction of the cortex and amygdala. *Infect. Immun.* **84**, 2861–2870 (2016).
10. C. N. David, E. S. Frias, J. I. Szu, P. A. Vieira, J. A. Hubbard, J. Lovelace, M. Michael, D. Worth, K. E. McGovern, I. M. Ethell, B. G. Stanley, E. Korzus, T. A. Fiacco, D. K. Binder, E. H. Wilson, GLT-1-Dependent Disruption of CNS Glutamate Homeostasis and Neuronal Function by the Protozoan Parasite Toxoplasma gondii. *PLoS Pathog.* **12**, 1–11 (2016).
11. J. M. Brooks, G. L. Carrillo, J. Su, D. S. Lindsay, M. A. Fox, I. J. Blader, Toxoplasma gondii infections alter GABAergic synapses and signaling in the central nervous system. *MBio*. **6**, e01428--15 (2015).
12. Y. Li, R. P. Viscidi, G. Kannan, R. McFarland, M. V. Pletnikov, E. G. Severance, R. H. Yolken, J. Xiao, Chronic Toxoplasma gondii Infection Induces Anti- N -Methyl-D-Aspartate Receptor Autoantibodies and Associated Behavioral Changes and Neuropathology. *Infect. Immun.* **86** (2018), doi:10.1128/IAI.00398-18.
13. I. Alsaady, E. Tedford, M. Alsaad, G. Bristow, S. Kohli, M. Murray, M. Reeves, M. S. Vijayabaskar, S. J. Clapcote, J. Wastling, G. A. McConkey, Downregulation of the Central Noradrenergic System by Toxoplasma gondii Infection. *Infect. Immun.* **87**, 567–98 (2018).
14. D. Samojłowicz, J. Twarowska-Małczyńska, A. Borowska-Solonynko, Ł. A.

Poniatowski, N. Sharma, M. Olczak, Presence of Toxoplasma gondii infection in brain as a potential cause of risky behavior: a report of 102 autopsy cases. *Eur. J. Clin. Microbiol. Infect. Dis.* **38**, 305–317 (2019).
15. J. Flegr, J. Havlícek, P. Kodym, M. Malý, Z. Smahel, Increased risk of traffic accidents in subjects with latent toxoplasmosis: a retrospective case-control study. *BMC Infect. Dis.* **2**, 11 (2002).
16. A. Nath, D. E. Hobson, A. Russell, Movement disorders with cerebral toxoplasmosis and AIDS. *Mov. Disord.* **8**, 107–12 (1993).
17. K. S. Burgdorf, B. B. Trabjerg, M. G. Pedersen, J. Nissen, K. Banasik, O. B. Pedersen, E. Sørensen, K. R. Nielsen, M. H. Larsen, C. Erikstrup, P. Bruun-Rasmussen, D. Westergaard, L. W. Thørner, H. Hjalgrim, H. M. Paarup, S. Brunak, C. B. Pedersen, E. F. Torrey, T. Werge, P. B. Mortensen, R. H. Yolken, H. Ullum, Large-scale study of Toxoplasma and Cytomegalovirus shows an association between infection and serious psychiatric disorders. *Brain. Behav. Immun.* **79**, 152–158 (2019).
18. P.-A. Witting, Learning capacity and memory of normal and Toxoplasma-infected laboratory rats and mice. *Z. Parasitenkd.* **61**, 29–51 (1979).
19. P. D. Gajewski, M. Falkenstein, J. G. Hengstler, K. Golka, Toxoplasma gondii impairs memory in infected seniors. *Brain. Behav. Immun.* **36**, 193–199 (2014).
20. B. P. Daniels, S. R. Sestito, S. T. Rouse, An expanded task battery in the Morris water maze reveals effects of Toxoplasma gondii infection on learning and memory in rats. *Parasitol. Int.* **64**, 5–12 (2015).
21. K. S. Rommelfanger, G. L. Edwards, K. G. Freeman, L. C. Liles, G. W. Miller, D. Weinshenker, Norepinephrine loss produces more profound motor deficits than MPTP treatment in mice. *Proc. Natl. Acad. Sci. U. S. A.* **104**, 13804–13809 (2007).
22. M. D. Marino, B. N. Bourdélat-Parks, L. Cameron Liles, D. Weinshenker, Genetic reduction of noradrenergic function alters social memory and reduces aggression in mice. *Behav. Brain Res.* **161**, 197–203 (2005).
23. R. D. Stowell, G. O. Sipe, R. P. Dawes, H. N. Batchelor, K. A. Lordy, B. S. Whitelaw, M. B. Stoessel, J. M. Bidlack, E. Brown, M. Sur, A. K. Majewska, Noradrenergic signaling in the wakeful state inhibits microglial surveillance and synaptic plasticity in the mouse visual cortex. *Nat. Neurosci.* **22**, 1782–1792 (2019).
24. Y. U. Liu, Y. Ying, Y. Li, U. B. Eyo, T. Chen, J. Zheng, A. D. Umpierre, J. Zhu, D. B. Bosco, H. Dong, L.-J. Wu, Neuronal network activity controls microglial process surveillance in awake mice via norepinephrine signaling. *Nat. Neurosci.* **22**, 1771–1781 (2019).
25. G. A. Laing, C., Blanchard, N., & McConkey, Noradrenergic Signaling-Neuroinflammation Cross-talk Regulates Toxoplasma gondii-Induced Behavioral Changes. *Trends Immunol. (in Press.* (2020).
26. H. H. Stibbs, Changes in brain concentrations of catecholamines and indoleamines in Toxoplasma gondii infected mice. *Ann. Trop. Med. Parasitol.* **79**, 153–7 (1985).
27. F. Haroon, U. Händel, F. Angenstein, J. Goldschmidt, P. Kreutzmann, H. Lison, K. D. Fischer, H. Scheich, W. Wetzel, D. Schlüter, E. Budinger, Toxoplasma gondii actively inhibits neuronal function in chronically infected mice. *PLoS One*. **7**, 1–16 (2012).
28. J. P. Dubey, L. R. Ferreira, M. Alsaad, S. K. Verma, D. A. Alves, G. N. Holland, G. A. McConkey, Experimental toxoplasmosis in rats induced orally with eleven strains of Toxoplasma gondii of seven genotypes: Tissue tropism, tissue cyst size, neural lesions, tissue cyst rupture without reactivation, and ocular lesions. *PLoS One*. **11**, 1–15 (2016).
29. S. Saayman, A. Ackley, A.-M. W. Turner, M. Famiglietti, A. Bosque, M. Clemson, V. Planelles, K. V Morris, An HIV-encoded antisense long noncoding RNA

epigenetically regulates viral transcription. *Mol. Ther.* **22**, 1164–1175 (2014).
30. A. Sinning, C. A. Hübner, Minireview: pH and synaptic transmission. *FEBS Lett.* **587**, 1923–1928 (2013).
31. G. A. McConkey, C. Peers, E. Prandovszky, Reproducing increased dopamine with infection to evaluate the role of parasite-encoded tyrosine hydroxylase activity. *Infect. Immun.* **83**, 3334–3335 (2015).
32. E. Tedford, thesis (2019).
33. T. Maeda, Y. Fukazawa, N. Shimizu, M. Ozaki, H. Yamamoto, S. Kishioka, Electrophysiological characteristic of corticoaccumbens synapses in rat mesolimbic system reconstructed using organotypic slice cultures. *Brain Res.* **1015**, 34–40 (2004).
34. M. Gissot, S.-W. Choi, R. F. Thompson, J. M. Greally, K. Kim, Toxoplasma gondii and Cryptosporidium parvum lack detectable DNA cytosine methylation. *Eukaryot. Cell*. **7**, 537–40 (2008).
35. A. A. Koshy, H. K. Dietrich, D. A. Christian, J. H. Melehani, A. J. Shastri, C. A. Hunter, J. C. Boothroyd, Toxoplasma co-opts host cells it does not invade. *PLoS Pathog.* **8**, 10–28 (2012).
36. C. Rodríguez-López, F. Clascá, L. Prensa, The Mesoaccumbens Pathway: A Retrograde Labeling and Single-Cell Axon Tracing Analysis in the Mouse. *Front. Neuroanat.* **11**, 25–31 (2017).
37. I. Potolicchio, G. J. Carven, X. Xu, C. Stipp, R. J. Riese, L. J. Stern, L. Santambrogio, Proteomic analysis of microglia-derived exosomes: metabolic role of the aminopeptidase CD13 in neuropeptide catabolism. *J. Immunol.* **175**, 2237–43 (2005).
38. E.-M. Kramer-Albers, N. Bretz, S. Tenzer, C. Winterstein, W. Mobius, H. Berger, K.-A. Nave, H. Schild, J. Trotter, Oligodendrocytes secrete exosomes containing major myelin and stress-protective proteins: Trophic support for axons? *Proteomics. Clin. Appl.* **1**, 1446–1461 (2007).
39. P. Sharma, P. Mesci, C. Carromeu, D. R. McClatchy, L. Schiapparelli, J. R. Yates, A. R. Muotri, H. T. Cline, Exosomes regulate neurogenesis and circuit assembly. *Proc. Natl. Acad. Sci. U. S. A.* **116**, 16086–16094 (2019).
40. S. Saeedi, S. Israel, C. Nagy, G. Turecki, The emerging role of exosomes in mental disorders. *Transl. Psychiatry*. **9**, 122 (2019).
41. R. Kalluri, V. S. LeBleu, The biology , function , and biomedical applications of exosomes. *Science (80-.).* **367**, 69–77 (2020).
42. C. Théry, K. W. Witwer, E. Aikawa, M. J. Alcaraz, J. D. Anderson, R. Andriantsitohaina, A. Antoniou, T. Arab, F. Archer, Minimal information for studies of extracellular vesicles 2018 (MISEV2018): a position statement of the International Society for Extracellular Vesicles and update of the MISEV2014 guidelines. *J. Extracell. Vesicles*. **7**, 1535750 (2018).
43. P. Sharma, P. Mesci, C. Carromeu, D. R. McClatchy, L. Schiapparelli, J. R. Yates, A. R. Muotri, H. T. Cline, Exosomes regulate neurogenesis and circuit assembly. *Proc. Natl. Acad. Sci.* **116**, 16086–16094 (2019).
44. T. C. Roberts, K. V. Morris, M. J. A. Wood, The role of long non-coding RNAs in neurodevelopment, brain function and neurological disease. *Philos. Trans. R. Soc. B Biol. Sci.* **369**, 20130507 (2014).
45. M. S. Weinberg, K. V. Morris, Transcriptional gene silencing in humans. *Nucleic Acids Res.* **44**, 6505–6517 (2016).
46. J. Fernandes, S. Acuña, J. Aoki, L. Floeter-Winter, S. Muxel, Long Non-Coding RNAs in the Regulation of Gene Expression: Physiology and Disease. *Non-Coding RNA*. **5**, 17 (2019).
47. C. Hewson, D. Capraro, J. Burdach, N. Whitaker, K. V. Morris, Extracellular vesicle

associated long non-coding RNAs functionally enhance cell viability. *Non-coding RNA Res.* **1**, 3–11 (2016).
48. E. B. Harrison, C. G. Hochfelder, B. G. Lamberty, B. M. Meays, B. M. Morsey, M. L. Kelso, H. S. Fox, S. V. Yelamanchili, Traumatic brain injury increases levels of miR-21 in extracellular vesicles: implications for neuroinflammation. *FEBS Open Bio*. **6**, 835–846 (2016).
49. P. G. Hawkins, S. Santoso, C. Adams, V. Anest, K. V. Morris, Promoter targeted small RNAs induce long-term transcriptional gene silencing in human cells. *Nucleic Acids Res.* **37**, 2984–2995 (2009).
50. M. Chivet, C. Javalet, K. Laulagnier, B. Blot, F. J. Hemming, R. Sadoul, Exosomes secreted by cortical neurons upon glutamatergic synapse activation specifically interact with neurons. *J. Extracell. vesicles*. **3**, 247–52 (2014).
51. Y. Yin, J. Y. Lu, X. Zhang, W. Shao, Y. Xu, P. Li, Y. Hong, L. Cui, G. Shan, B. Tian, Q. C. Zhang, X. Shen, U1 snRNP regulates chromatin retention of noncoding RNAs. *Nature*. **580**, 147–150 (2020).
52. D. J. Chandler, P. Jensen, J. G. McCall, A. E. Pickering, L. A. Schwarz, N. K. Totah, Redefining Noradrenergic Neuromodulation of Behavior: Impacts of a Modular Locus Coeruleus Architecture. *J. Neurosci.* **39**, 8239–8249 (2019).
53. K. L. Menard, B. E. Haskins, A. P. Colombo, E. Y. Denkers, Toxoplasma gondii Manipulates Expression of Host Long Noncoding RNA during Intracellular Infection. *Sci. Rep.* **8**, 15017 (2018).
54. S. A. Hari Dass, A. Vyas, Toxoplasma gondii infection reduces predator aversion in rats through epigenetic modulation in the host medial amygdala. *Mol. Ecol.* **23**, 6114–22 (2014).
55. T. Takeuchi, A. J. Duszkiewicz, A. Sonneborn, P. A. Spooner, M. Yamasaki, M. Watanabe, C. C. Smith, G. Fernández, K. Deisseroth, R. W. Greene, R. G. M. Morris, Locus coeruleus and dopaminergic consolidation of everyday memory. *Nature*. **537**, 357–362 (2016).
56. E. Prandovszky, E. Gaskell, H. Martin, J. P. Dubey, J. P. Webster, G. A. McConkey, The neurotropic parasite Toxoplasma gondii increases dopamine metabolism. *PLoS One*. **6**, 1–23 (2011).
57. J. Martynowicz, L. Augusto, R. C. Wek, S. L. Boehm, W. J. Sullivan, Guanabenz Reverses a Key Behavioral Change Caused by Latent Toxoplasmosis in Mice by Reducing Neuroinflammation. *MBio*. **10** (2019), doi:10.1128/mBio.00381-19.
58. M.-J. Gubbels, C. Li, B. Striepen, High-Throughput Growth Assay for Toxoplasma gondii Using Yellow Fluorescent Protein. *Antimicrob. Agents Chemother.* **47**, 309–316 (2003).
59. B. A. Fox, A. Falla, L. M. Rommereim, T. Tomita, J. P. Gigley, C. Mercier, M.-F. Cesbron-Delauw, L. M. Weiss, D. J. Bzik, Type II Toxoplasma gondii KU80 knockout strains enable functional analysis of genes required for cyst development and latent infection. *Eukaryot. Cell*. **10**, 1193–206 (2011).
60. R. A. Dielenberg, G. E. Hunt, I. S. McGregor, When a rat smells a cat: The distribution of Fos immunoreactivity in rat brain following exposure to a predatory odor. *Neuroscience*. **104**, 1085–1097 (2001).
61. B. M. Filippi, M. A. Abraham, P. N. Silva, M. Rasti, M. P. LaPierre, P. V Bauer, J. V Rocheleau, T. K. T. Lam, Dynamin-Related Protein 1-Dependent Mitochondrial Fission Changes in the Dorsal Vagal Complex Regulate Insulin Action. *Cell Rep.* **18**, 2301–2309 (2017).
62. A. Matevossian, S. Akbarian, Neuronal nuclei isolation from human postmortem brain tissue. *J. Vis. Exp.* **9**, 1–21 (2008).

63. M. A. Livshits, E. Khomyakova, E. G. Evtushenko, V. N. Lazarev, N. A. Kulemin, S. E. Semina, E. V. Generozov, V. M. Govorun, Isolation of exosomes by differential centrifugation: Theoretical analysis of a commonly used protocol. *Sci. Rep.* **5**, 17319 (2015).
64. R. P. Alexander, N.-T. Chiou, K. M. Ansel, Improved exosome isolation by sucrose gradient fractionation of ultracentrifuged crude exosome pellets. *Protoc. Exch.* **11**, 1–9 (2016).
65. Y. Wu, W. Deng, D. J. Klinke, II, Exosomes: improved methods to characterize their morphology, RNA content, and surface protein biomarkers. *Analyst*. **140**, 6631–42 (2015).
66. J. Sambrook, D. W. Russell, Purification of nucleic acids by extraction with phenol:chloroform. *CSH Protoc.* **6**, 44–55 (2006).
67. T. C. Roberts, J. R. Hart, M. U. Kaikkonen, M. S. Weinberg, P. K. Vogt, K. V Morris, Quantification of nascent transcription by bromouridine immunocapture nuclear run-on RT-qPCR. *Nat. Protoc.* **10**, 1198–211 (2015).
68. C. Théry, S. Amigorena, G. Raposo, A. Clayton, Isolation and Characterization of Exosomes from Cell Culture Supernatants and Biological Fluids. *Curr. Protoc. Cell Biol.* **30**, 3221–29 (2006).
69. G. Paxinos, C. Watson, *The Rat Brain in Stereotaxic Coordinates* (Academic Press, ed. 6th, 2009).
70. A. R. Gruber, R. Lorenz, S. H. Bernhart, R. Neuböck, I. L. Hofacker, The Vienna RNA websuite. *Nucleic Acids Res.* **36**, W70-4 (2008).

Acknowledgements

The authors wish to thank Mohammad Alsaad and Steve Clapcote who performed mouse infections, dissection and cryostat sectioning, and Greg Bristow who performed rat infections and tissue collection. We thank Dong Xia for the proteomic analysis of the EVs. Additionally, Martin Fuller for electron microscopy and Agne Antanaviciute performed Methylseq genome analysis. FACS was performed with the assistance of Sally Boxall at the Cell Sorting Facility of the University of Leeds.

Ethics Declaration
The authors declare no competing interests.

FIGURES

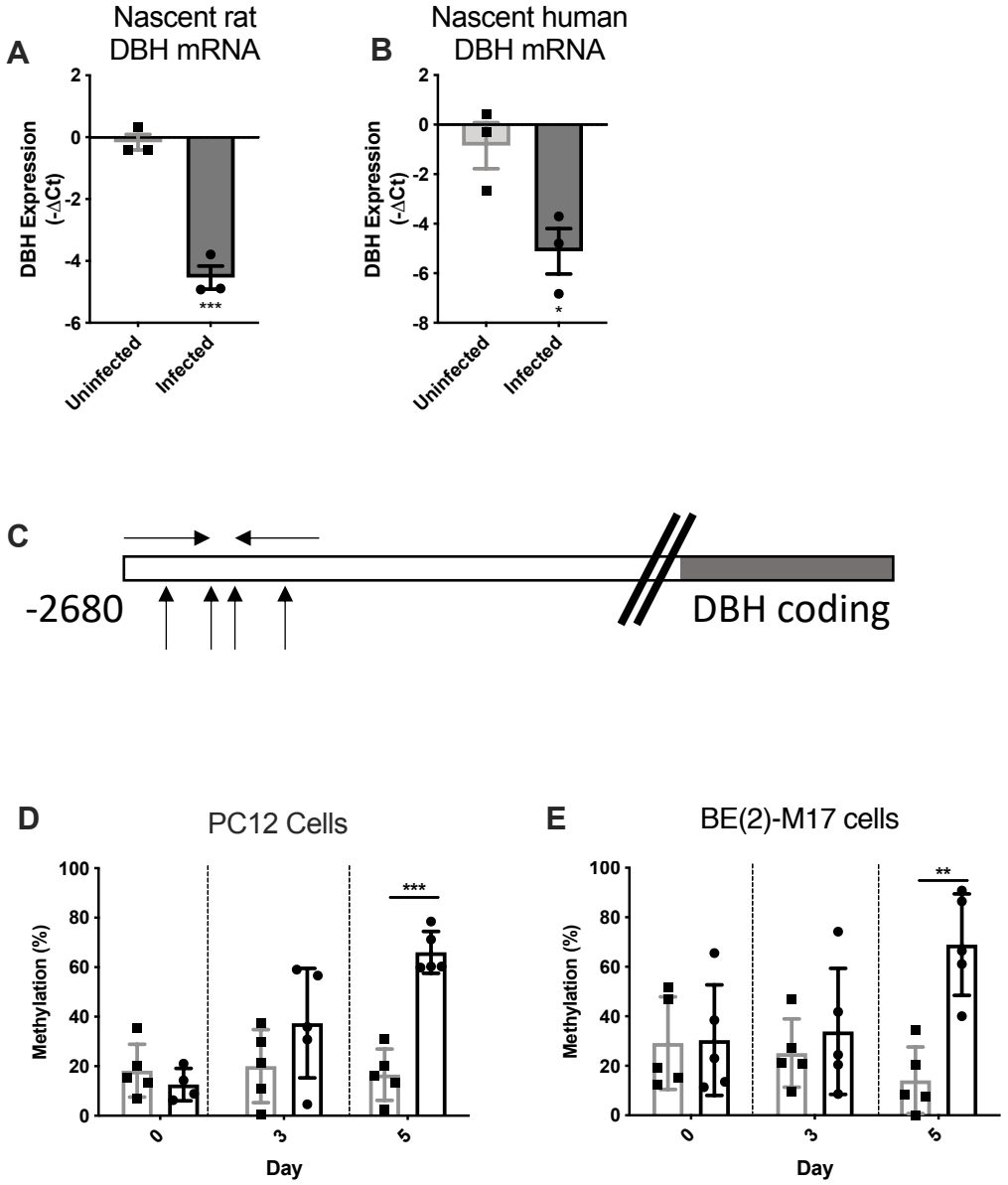

Figure 1: Transcription of the DBH gene is transcriptionally regulated during *T. gondii* infection. A) Nascent *DBH* pre-mRNA transcription (relative to GAPDH) in catecholaminergic PC12 cells infected with pH-shocked parasites. After 5 days of infection nuclear run-on assays were performed. MOI 1; n=5; ***p<0.001. **B)** Nascent *DBH* expression in uninfected and infected human neuronal cells as in (A). Multiplicity of infection (MOI) 1; n=3, *p<0.05. **C)** Diagram depicting the *DBH* promoter analysis by Methylation Sensitive Restriction Enzyme qPCR (MSRE-qPCR). The DBH coding region is shaded grey. The location of the methylation sensitive restriction enzyme sites are shown with up arrows and the

primer sites with facing arrows (not to scale). **D)** *DBH* promoter methylation was measured by MSRE-qPCR. Percentage of methylation in the 5' promoter region of the *DBH* gene in PC12 cells was measured by MSRE qPCR as in Fig 3. DNA was collected at 0, 3 and 5 days of infection from uninfected (grey) or infected (black) rat catecholaminergic cells. MOI=1; n=5, ***p= 0.0007. **E)** Methylation measured as in (A) during course of infection for human neuronal (BE(2)-M17) cells. MOI=1; n=5, **p= 0.0011. Unpaired Student t tests, ± SEM shown.

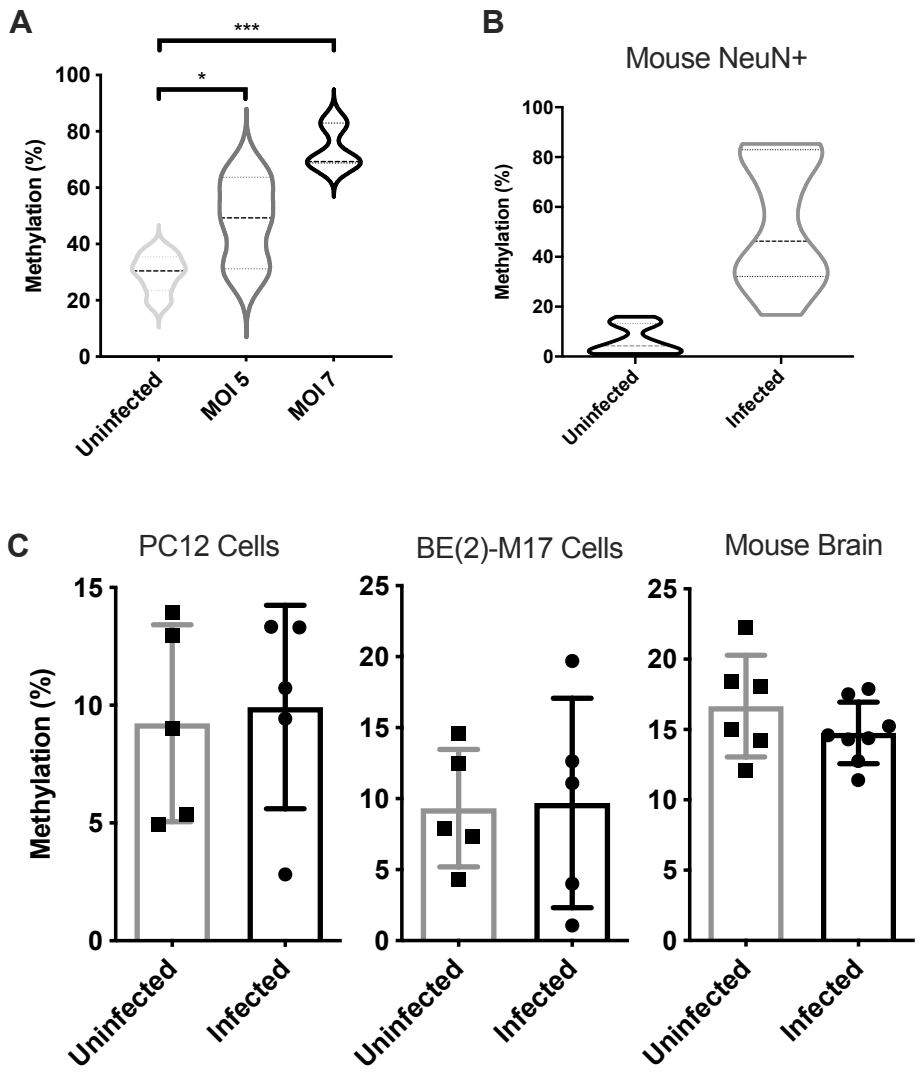

Figure 2: Hypermethylation of the DBH promoter region during infection despite no change in global methylation patterns. A) *DBH* promoter methylation was measured by MSRE-qPCR in organotypic coronal midbrain section cultures. Slice cultures were either uninfected (light grey, n=6) or infected with wild-type induced-bradyzoite *T. gondii* at MOI 5 (dark grey, n=3) and MOI 7 (black, n=3). Infection was monitored for 5 days by light microscopy; n=3 biological repeats containing 3 slices from the same rat per well, * p=0.04, *** p= 0.000051 shown. One-way ANOVA, p= 0.0005 Tukey's post hoc test MOI 7 vs uninfected p=0.0004. **B)** Methylation at the *DBH* promoter region in neurons from uninfected (grey, n=9) and chronically-infected (black, n=11) mice. Neurons were enriched from harvested brains by FACS using NeuN antibody and *DBH* methylation quantified by MSRE-qPCR. p=0.0004. **C)** Total DNA methylation measured by ELISA of both uninfected and infected rat catecholaminergic PC12 cells (n=3, p=0.52), human neuronal BE(2)-M17 cell (n=5, 0.59) and neuronal nuclei enriched by FACS from mouse brain tissue for uninfected (n=6) and chronically-infected mice (n=3, p=0.15). No significant change in methylation was identified by Student t tests, ± SEM shown.

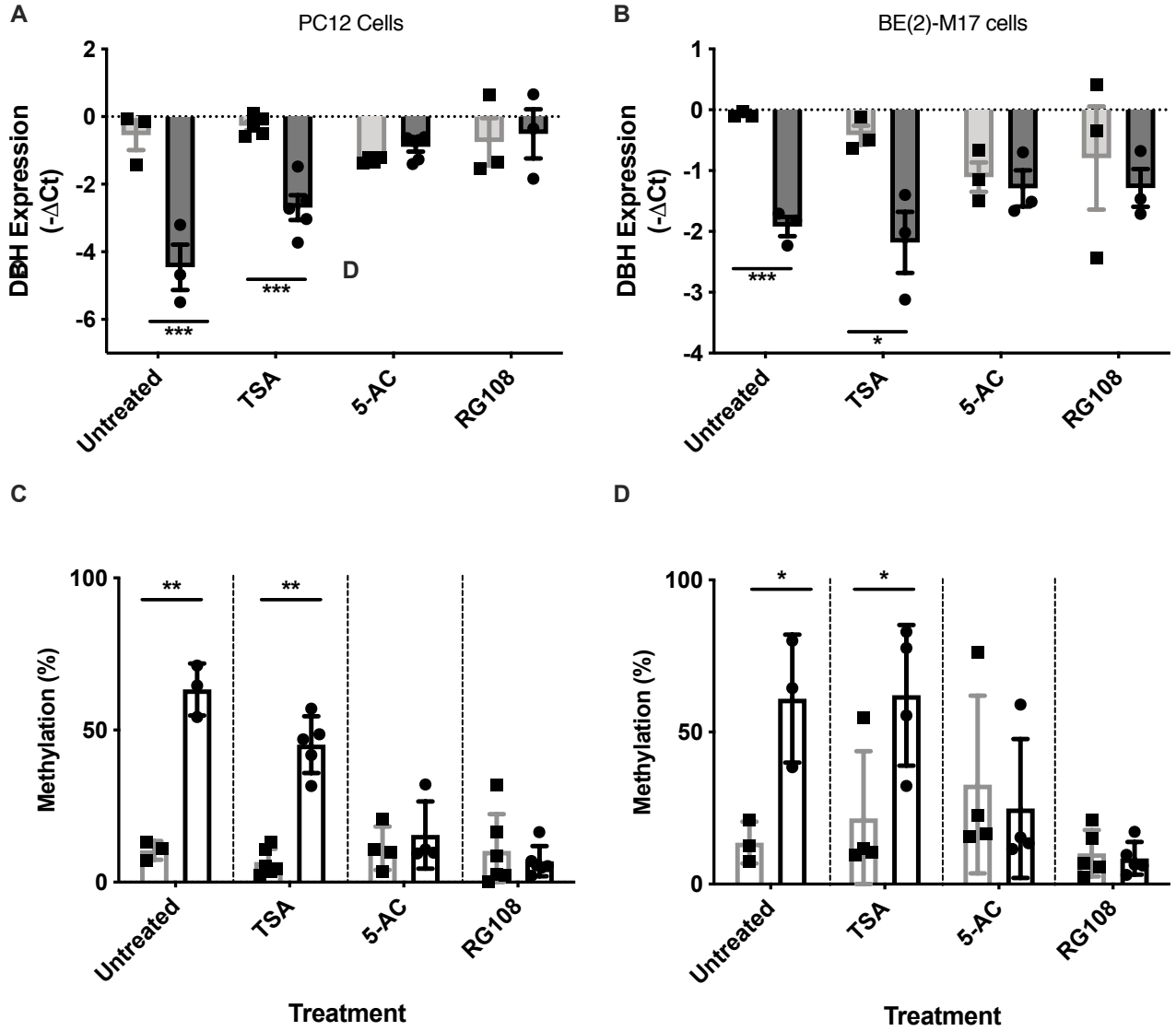

Figure 3: *DBH* transcriptional regulation changes are abrogated in cells treated with histone deacetylase and DNA methyltransferase inhibitors. A) Expression of *DBH* mRNA measured by RT-qPCR relative to GAPDH. Uninfected (grey) and *T. gondii*-infected (black) rat catecholaminergic PC12 cells treated with trichostatin A (TSA), 5-azacytidine (5-AC) and RG108; n=5, ** $p<0.01$. **B)** As in (A) with neuronal BE(2)-M17 cells treated with TSA, 5-AC and RG108; n=5, * $p<0.05$. n=5. Student t test, ±SEM shown. **C)** 5' DBH promoter hypermethylation was measured via MSRE qPCR (as above) and methylation expressed as a percentage. Uninfected (grey) and T. gondii-infected (black) rat PC12 cells treated with trichostatin A (TSA), 5-azacytidine (5-AC) and RG108; n=5, ** $p<0.01$. **D)** Uninfected (grey) and infected (black) human neuronal BE(2)-M17 cells treated as in (A) with TSA, 5-AC and RG108; n=5, * $p<0.05$. Student t test, ±SEM shown.

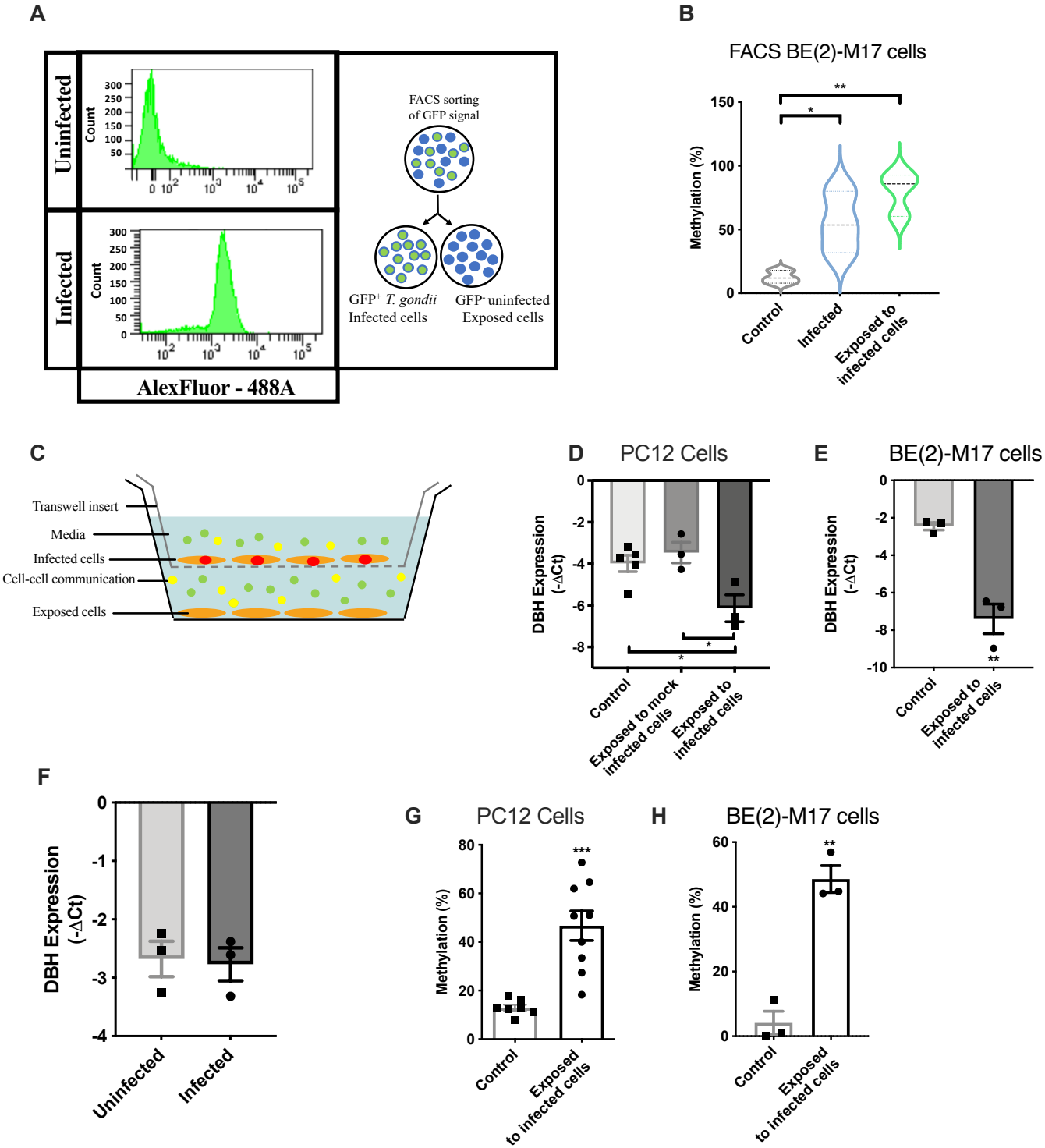
A
Uninfected
Infected
Count
AlexFluor - 488A
FACS sorting
of GFP signal
GFP+ T. gondii
Infected cells
GFP- uninfected
Exposed cells
B
FACS BE(2)-M17 cells
Methylation (%)
Control
Infected
Exposed to
infected cells
C
Transwell insert
Media
Infected cells
Cell-cell communication
Exposed cells
D
PC12 Cells
DBH Expression
(-ΔCt)
Control
Exposed to mock
infected cells
Exposed to
infected cells
E
BE(2)-M17 cells
DBH Expression
(-ΔCt)
Control
Exposed to
infected cells
F
DBH Expression
(-ΔCt)
Uninfected
Infected
G
PC12 Cells
Methylation (%)
Control
Exposed
to infected cells
H
BE(2)-M17 cells
Methylation (%)
Control
Exposed
to infected cells

Figure 4: Noradrenergic cells infected with bradyzoite-like *T. gondii* secrete a signalling factor. A) Representative plot showing cell count against GFP signal for FACs of GFP-negative uninfected, exposed cells and GFP positive cells infected with GFP-expressing parasites. Right panel shows a schematic representation of experimental design. Human neuronal BE(2)-M17 cells were infected with bradyzoite-induced *T. gondii*, after 5 days of infection FACS was performed and DNA was then harvested. MSRE qPCR was utilised to measure *DBH* promoter methylation. **B)** Methylation at the 5' prime *DBH* promoter region of FACS sorted BE(2)-M17 cells measured using MSRE qPCR; n=3, * $p<0.05$, ** $p<0.01$ shown. One-way ANOVA, p= 0.0089, Tukey's post hoc test exposed to infected cells vs control p=0.0077. **C)** Scheme of transwell culture system with human foreskin fibroblasts (HFF cells) infected with *T. gondii* on the top layer and human neuronal BE(2)-M17 cells on the bottom layer separated by a 0.4µm membrane. Cells are orange, parasites red, signalling factors in vesicles (green) and soluble (yellow). **D)** *DBH* expression measured using RT-qPCR (relative to GAPDH) in rat catecholaminergic PC12 cells cultured in a transwell with either uninfected control, *T. gondii* infected or mock-infected cells in the upper transwell layer; RNA was harvested from cells in the lower transwell after 5 days. Mock infected cells were incubated with heat-killed *T. gondii* tachyzoites n=3, * $p<0.05$. One-way ANOVA p= 0.017, Tukey's post hoc test uninfected and mock-infected vs infected p=0.020 and p=0.033, respectively. **E)** Human neuronal BE(2)-M17 cell expression of *DBH* mRNA cultured in transwells and treated as in (B); n=3, p=0.0038. **F)** The permeable factors released from infected fibroblasts did not change *DBH* expression levels in exposed noradrenergic cells. RNA was harvested and RT-qPCR performed on the BE(2)-M17 cells after 5 days of infection. Plot shows *DBH* mRNA relative to the reference gene *GAPDH*. *DBH* gene expression was not significantly altered by exposure to infected fibroblasts (p=0.84); ±SEM shown, n=3, Student t test. **G)** Percentage 5' DBH promoter region methylation plotted of PC12 cells cultured with uninfected or 5-day bradyzoite-induced *T. gondii* infected cells on the upper transwell layer. ±SEM shown, n=3, Student t test, ** $p<0.01$. **H)** M17 cell DBH promoter methylation measured via MSRE qPCR. M17 cells were cultured with either uninfected (n=4) or 5 day T. gondii infected M17 cells (n=9). ±SEM shown, Student t test, *** $p<0.001$.

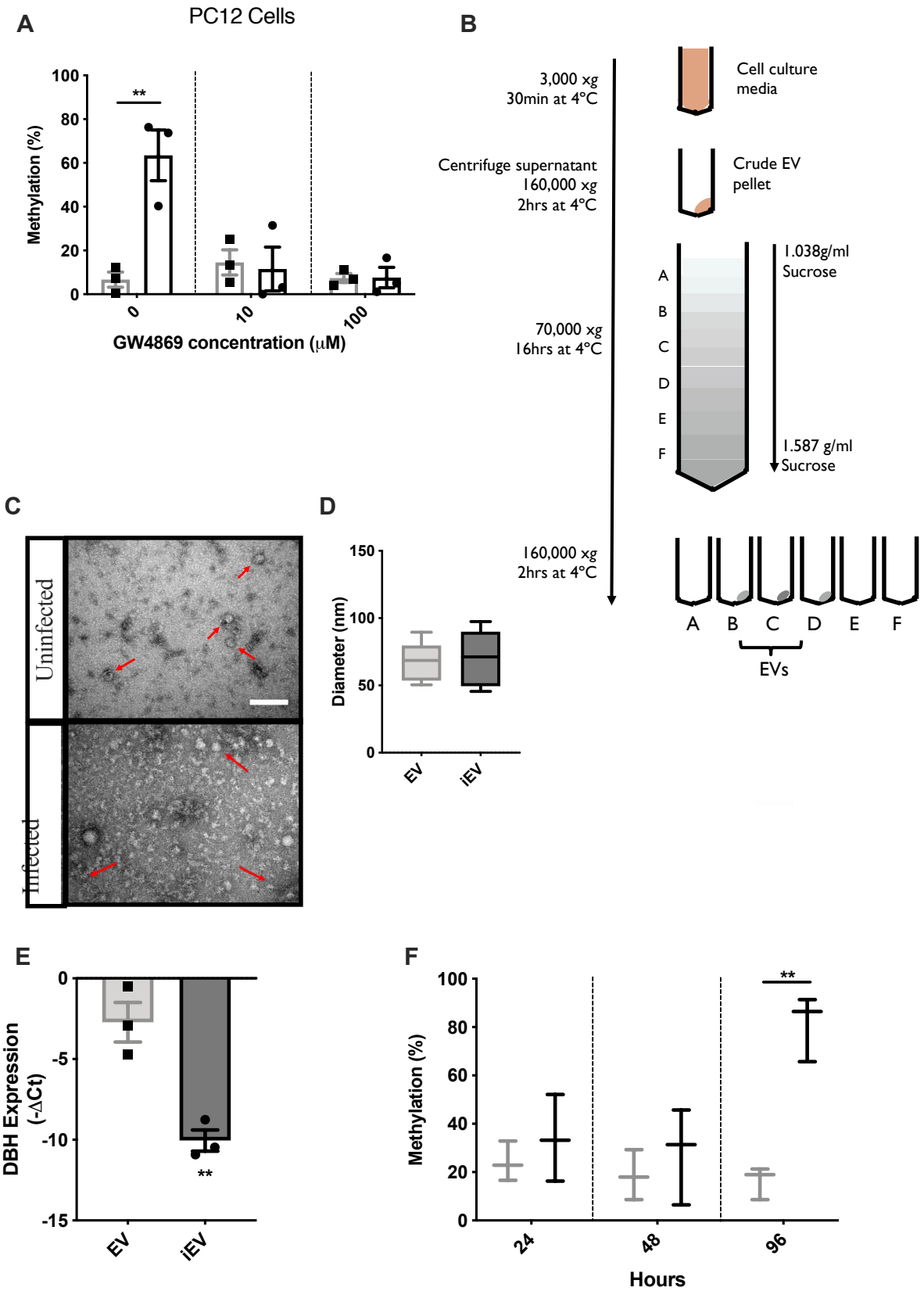
A
PC12 Cells
Methylation (%)
100
80
60
40
20
0
**
0
10
100
GW4869 concentration (μM)
B
3,000 xg
30min at 4°C
Cell culture
media
Centrifuge supernatant
160,000 xg
2hrs at 4°C
Crude EV
pellet
70,000 xg
16hrs at 4°C
1.038g/ml
Sucrose
A
B
C
D
E
F
1.587 g/ml
Sucrose
160,000 xg
2hrs at 4°C
A B C D E F
EVs
C
Uninfected
Infected
D
Diameter (nm)
150
100
50
0
EV
iEV
E
DBH Expression
(-ΔCt)
0
-5
-10
-15
**
EV
iEV
F
Methylation (%)
100
80
60
40
20
0
**
24
48
96
Hours

Figure 5: Extracellular vesicles induce transcriptional regulation and epigenetic changes in neuronal cells. A) PC12 cells in the lower layer were exposed to uninfected (grey) or *T. gondii*-infected (black) PC12 cells in the upper layer of a transwell system in media supplemented with 0µM, 10µM or 100µM of GW4869, a neutral sphingomyelinase (N-SMase) inhibitor. DBH promoter methylation in the exposed cells was quantified by MSRE qPCR as above. ± SEM shown, n=3, Student t test, ** p=0.0093. **B)** Scheme summarising sequential ultracentrifugation steps undertaken to produce purified extracellular vesicles. Sucrose gradient densities range from 0.104 g/ml to 1.43 g/ml. The density between 1.15 and 1.19 g/ml is collected as this represents extracellular vesicles (*68*). **C)** Transmission electron microscopy of extracellular vesicles isolated from uninfected (top) and infected (bottom) PC12 cells. Arrows indicate extracellular vesicles; scale bar represents 100nm. **D)** Plot of extracellular vesicle diameter from uninfected (EV) and *T. gondii* infected PC12 cells (iEV); as measured by ImageJ; n=10, p=0.81 **E)** *DBH* mRNA expression following treatment with purified extracellular vesicles. PC12 cells were treated EVs from uninfected (grey) and *T. gondii* infected (black) PC12 cells for 24 hours; n=3, ** p=0.006. Graphs shown ±SEM with p values for student t tests. **F)** Time course of methylation changes induced by EV treatment. Percentage methylation of the 5' *DBH* promoter region in cells treated every 24 hours with extracellular vesicles purified from uninfected (grey) or 5 day *T. gondii* infected (black) PC12 cells. DNA was harvested after 24, 48 and 96 hours of treatment; the minimum and maximum shown with line indicating mean; n=3, **p=0.0018. Graphs shown ±SEM with p values for Student t tests.

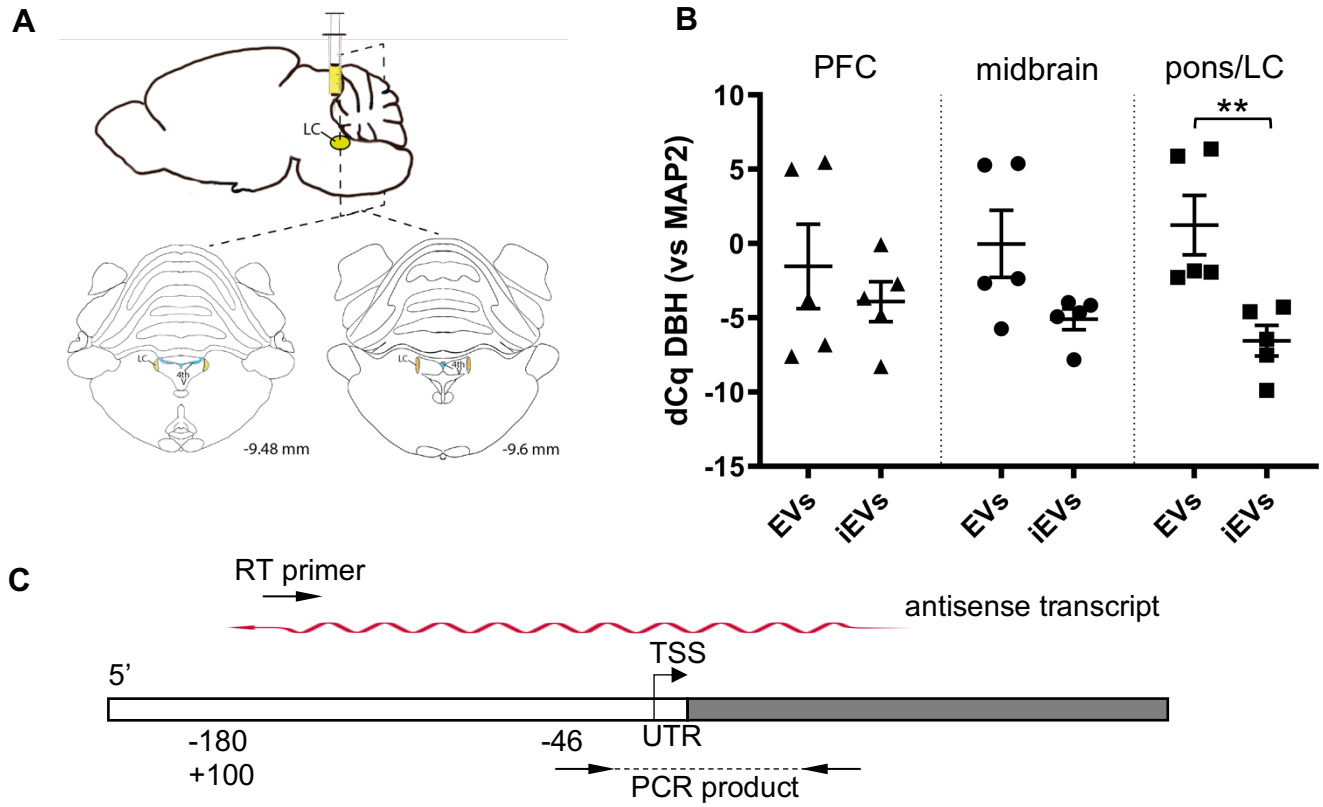
A
LC
-9.48 mm
-9.6 mm
B
PFC
midbrain
pons/LC
**
dCq DBH (vs MAP2)
10
5
0
-5
-10
-15
EVs
iEVs
EVs
iEVs
EVs
iEVs
C
RT primer
antisense transcript
TSS
5'
-180
+100
-46
UTR
PCR product

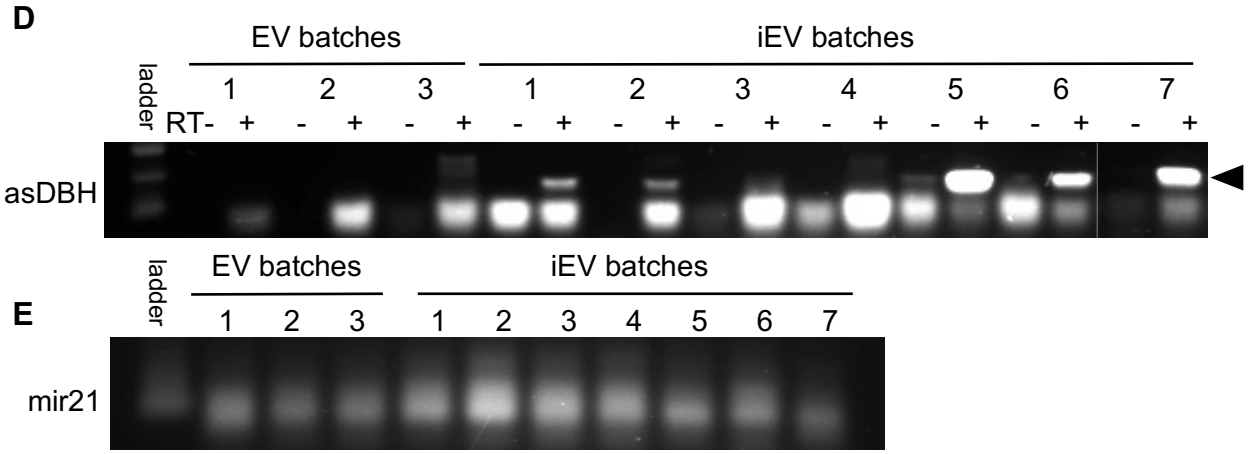
D
EV batches
iEV batches
ladder
1 2 3 1 2 3 4 5 6 7
RT- + - + - + - + - + - + - + - + - + - +
asDBH
E
ladder
EV batches
iEV batches
1 2 3 1 2 3 4 5 6 7
mir21

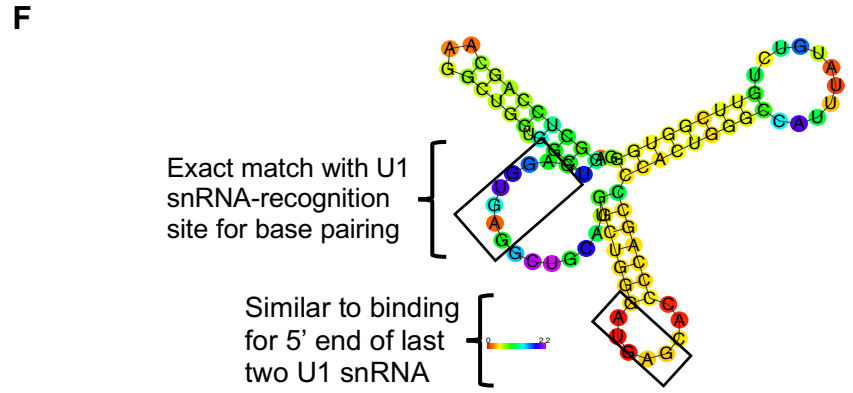
F
Exact match with U1 snRNA-recognition site for base pairing
Similar to binding for 5' end of last two U1 snRNA

Figure 6: Extracellular vesicles from infected cells contain a *DBH* lncRNA and down-regulate *DBH* in rat brains. A) A schematic representation of experimental design illustrating site of injection for delivery of extracellular vesicles purified from uninfected or *T. gondii*-infected rat catecholaminergic PC12 cultures into the locus coeruleus of Sprague-Dawley rats. Treatment was twice daily for 3 days via a cannula. Brains were harvested 45 hours following the final injection and sectioned to separate the prefrontal cortex, midbrain containing the hippocampus, and the hindbrain containing the locus coeruleus, as illustrated by the dotted lines. RNA was purified from tissues and RT-qPCR performed to quantitate *DBH* expression. Stereotaxic coordinates from Paxinos and Watson (*69*). **B)** *DBH* mRNA levels in brain tissues of rat receiving extracellular vesicles purified from uninfected (EVs) or *T. gondii*-infected (iEVs) cultures relative to neuronal marker MAP2. The pons containing locus coeruleus (pons/LC) has higher *DBH* than the prefrontal cortex (PFC) or midbrain. ±SEM shown, n=5, Mann-Whitney unpaired t test, ** p=0.0079. **C)** Schematic representation of the *DBH* gene. The transcription start site (TSS) and untranslated region are highlighted with the binding sites of the directional RT and PCR primers used to detect the antisense ncRNA. The antisense lncRNA is depicted as the undulating arrow. **D)** Detection of the *DBH* antisense ncRNA (asDBH) as determined by directional reverse transcription and PCR. The products from biological repeats of EVs from infected PC12 cultures (n=7) and EVs from uninfected cultures (n=3) are shown. The 138 bp product (arrowhead) is indicated, faint in some lanes, was verified by sequencing and a spurious band is visible in some lanes. Alternating lanes on the agarose gel are controls lacking reverse transcriptase (RT). The full gel photo is shown in **Fig. S**8. A 1 kb Plus DNA Ladder (NEB) is the first lane. **E)** As a control for RNA quality of samples, miR-21 was amplified by RT-PCR from all samples. **F)** Minimum free energy secondary structure prediction of DBH lncRNA with the base pair probabilities shown using RNAfold (*70*). The drawing shows the conserved U1 snRNA-recognition site by base pairing in a stem loop (upper box). Bases similar to binding for 5' end of U1 snRNA as described in Yin et al are also found in a loop region (lower box) (*51*). Top hits for minimum free energy structure predictions with other algorithms (e.g. Predict a Secondary Structure Web Server by the Matthews lab, Rochester) also place the U1-recognition site in a stem loop.

SUPPLEMENTAL FIGURES

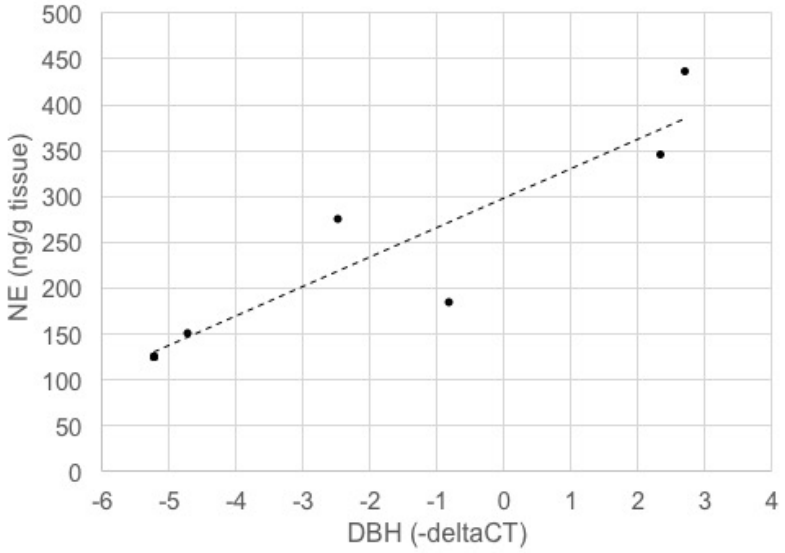

Supplemental Fig 1. Dopamine beta-hydroyxlase directly correlates with norepinephrine (NE) levels in rat brains. Norepinephrine levels were measured by HPLC and dopamine beta-hydroxylase (DBH) was quantitated by RT-qPCR (relative to GAPDH) in brain tissue from rats. The Pearson's correlation coefficient is 0.81 and the R value is 0.90 with a p value of 0.014.

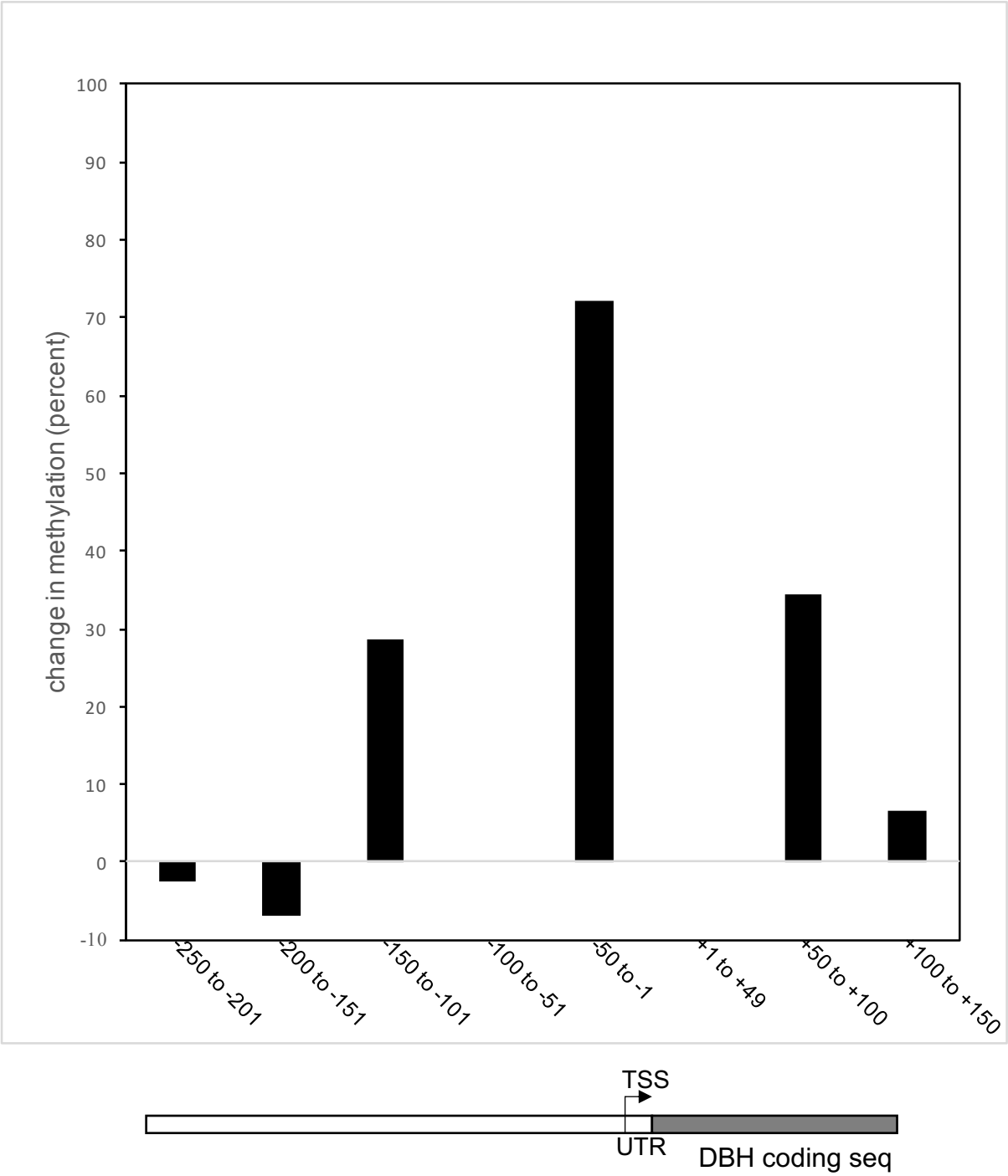

Supplemental Data Fig. 2. Methylation in the *DBH* upstream region based on bisulfite sequencing. Graph depicting the changes in CpG methylation across the *DBH* gene region from massive parallel genome sequencing for infected noradrenergic PC12 cells from three infected and three uninfected cultures at day five of *T. gondii* infection.

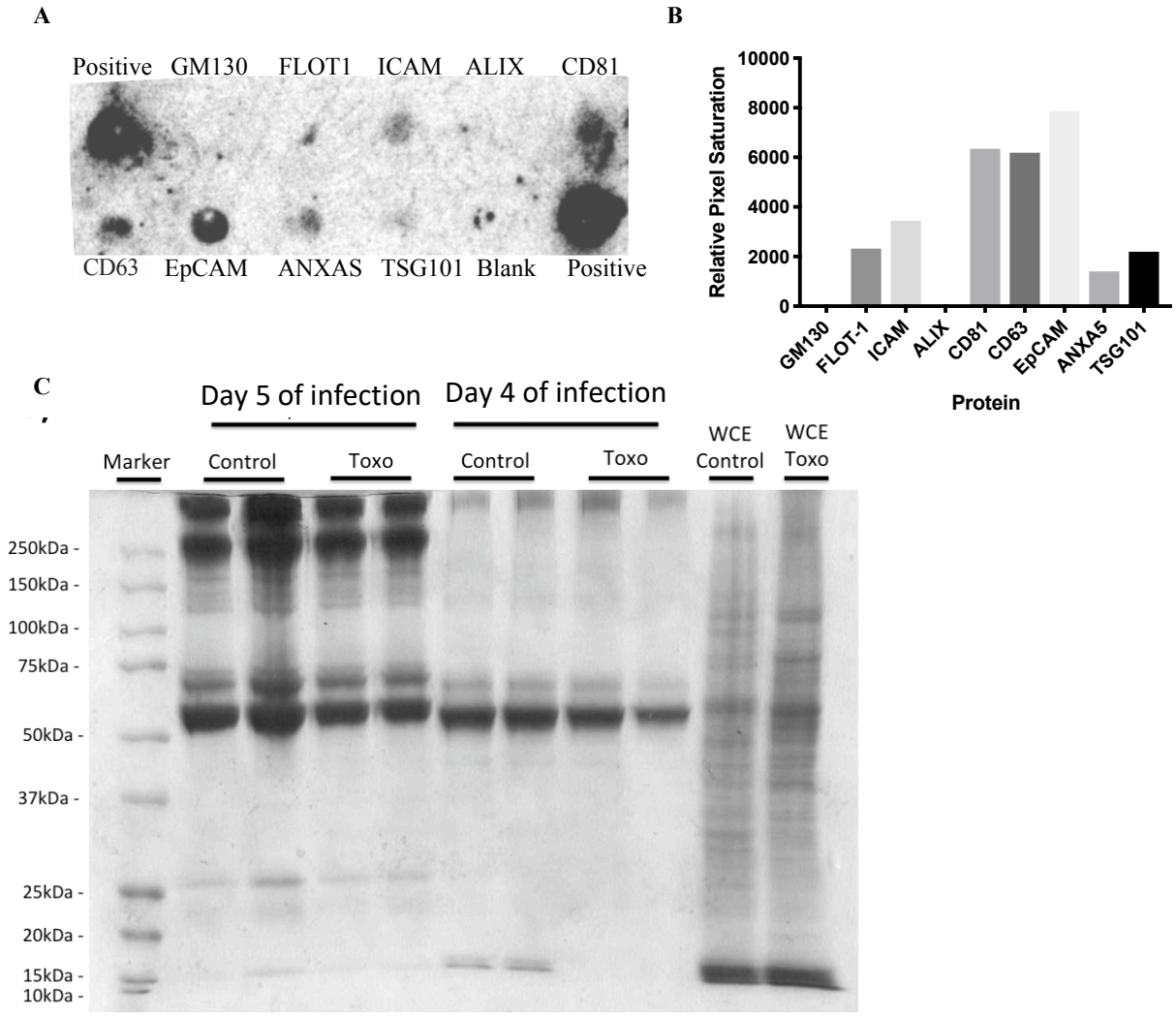

Supplemental Data Fig. 3: Extracellular vesicles isolated from infected cells exhibit classical exosomal markers. A) Image of a commercial dot blot probed with protein (300µg) from purified extracellular vesicles from *T. gondii* infected rat catecholaminergic cells. The dot blot contained eight common exosome markers and GM130 to indicate cellular contamination. (Exo-Check™ Exosome Antibody Array, System Biosciences, Palo Alto) with upper left and lower right HRP-conjugated antibody as positive controls. **B)** Quantitation of luminescence in the blot of the exosome markers using imageJ software. **C)** Protein analysis of EVs isolated from PC12 cells and infected cells. Purified protein from EVs was resolved by 12% SDS-PAGE and a coomassie blue stained image is shown. Protein markers and control whole cell extracts (WCE) are shown. The yield of purified EVs was not significantly different between infected and uninfected (control) cultures after four days (t-test, $n = 4$, $p > 0.05$) or five days (t-test, $n = 4$, $p > 0.05$) of infection (data not shown).

A

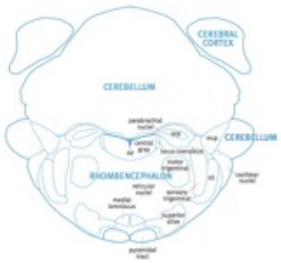

B

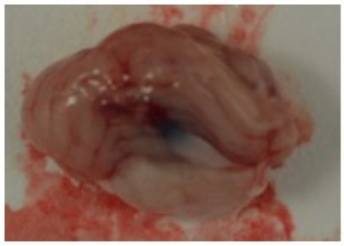

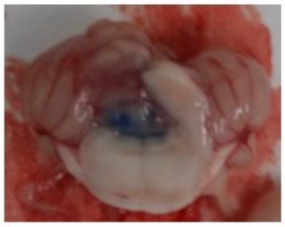

Supplemental Data Fig. 4. Delivery of EVs to the locus coeruleus. A) Diagram of coronal section of the rat hindbrain taken from Paxinos and Watson, Academic Press **The Rat Brain in Stereotaxic Coordinates 6th ed. B)** Examples of hindbrains dissected from rats shows localization of EV delivery by the bromophenol blue dye delivered through the cannula.

A

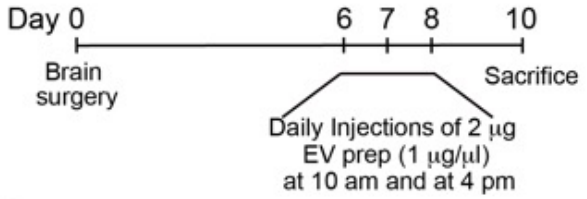
Day 0
6 7 8
10
Brain surgery
Sacrifice
Daily Injections of 2 μg EV prep (1 μg/μl) at 10 am and at 4 pm

B

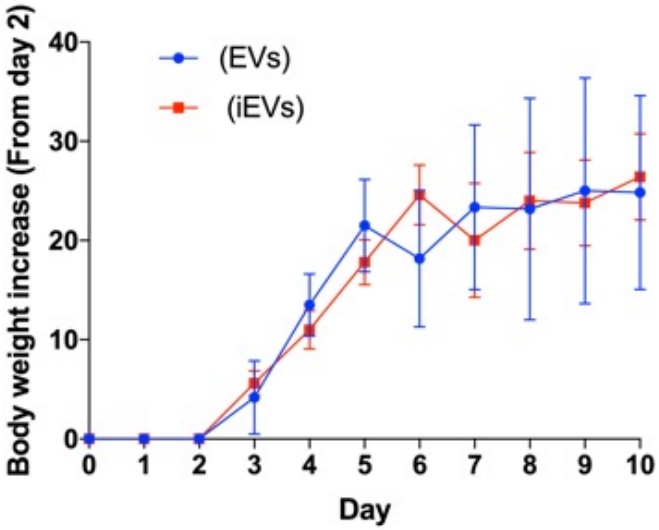
Body weight increase (From day 2)
(EVs)
(iEVs)
Day

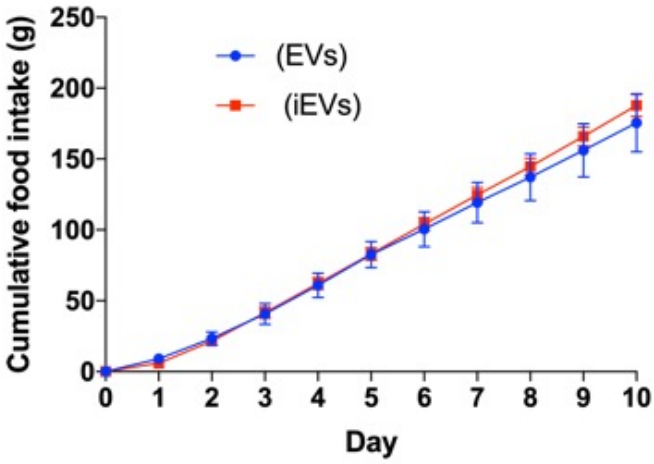
Cumulative food intake (g)
(EVs)
(iEVs)
Day

C

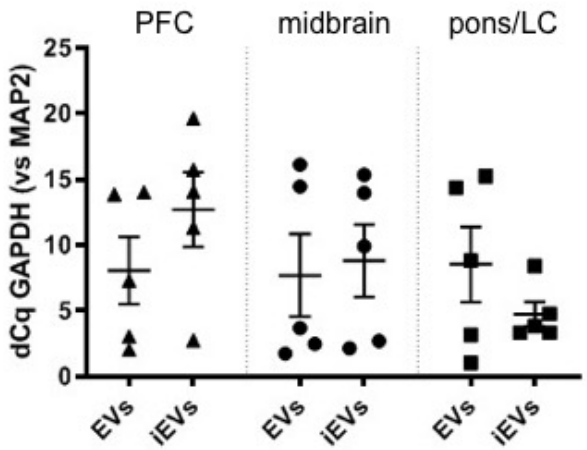
PFC
midbrain
pons/LC
dCq GAPDH (vs MAP2)
EVs
iEVs
EVs
iEVs
EVs
iEVs

Supplemental Data Fig. 5. Intracerebral injection of extracellular vesicles (EVs) effect on health status and brain GAPDH expression. A) Timeline of the protocol for intracranial treatment of rats with purified EVs **B)** Body weight and appetite, measured as food consumption, in animals; during the course of the experiment. Following recovery from surgery these are normal. **C)** Expression of GAPDH in brain cells following EV treatment. Rats received EVs purified from uninfected or *T. gondii*-infected (iEVs) cultures. Brains were sectioned into the prefrontal cortex (PFC), midbrain, and the hindbrain containing the locus coeruleus (pons/LC). Expression of GAPDH, as a representative gene for numbers of astrocytes, oligodendrocytes, microglia, and neurons shown relative to the neuronal marker MAP2. dCq is difference in Cq quantification cycle between GAPDH and MAP2, ±SEM shown, n=5, Student t test iEVs vs EVs for the regions p = 0.86, 0.28, and 0.26, respectively.

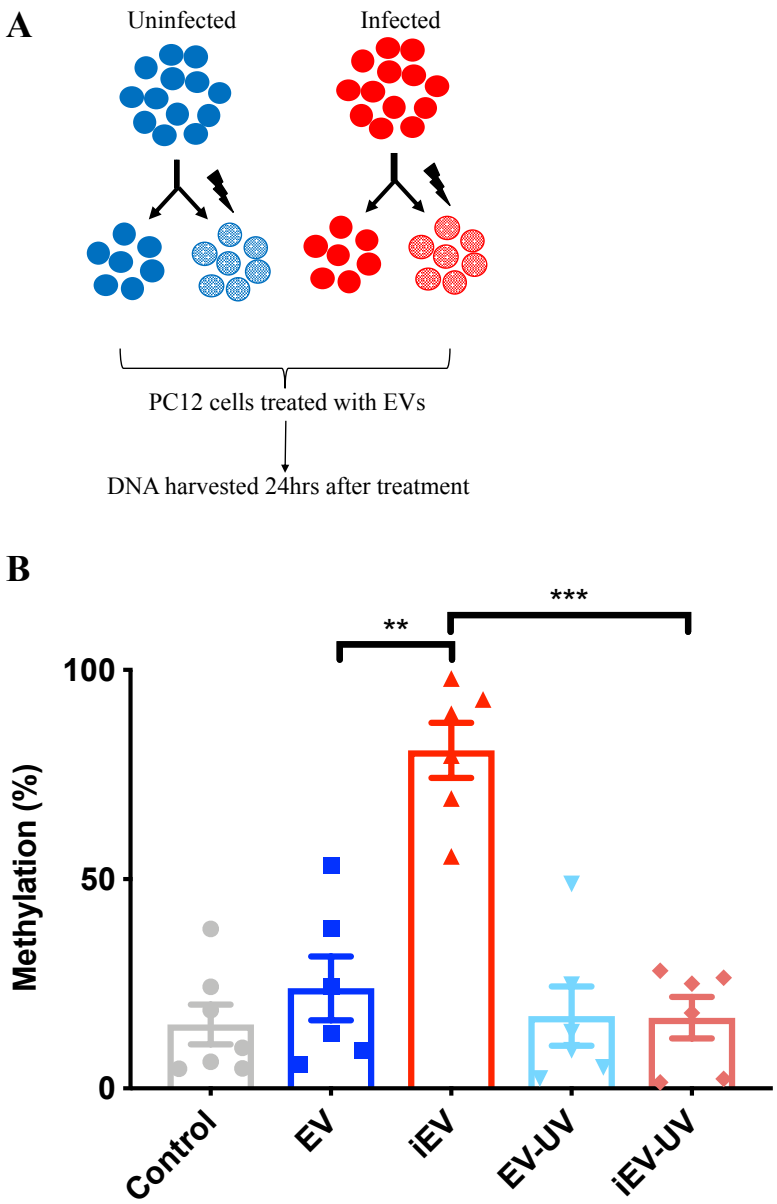

Supplemental Data Fig. 6: UV irradiation reverses the effect of infection-derived EVs on 5' promoter methylation of *DBH*. A) A schematic representation of experimental design. EVs purified from uninfected or *T. gondii*-infected rat catecholaminergic PC12 cells were mock or UV irradiated for 10 minutes at 4°C. PC12 cells were incubated with the EVs for three days and DNA harvested. **B)** Percentage methylation of the 5' promoter region of *DBH* was measured by MSRE qPCR. PC12 cells were untreated (grey) or treated with EVs purified from uninfected cells and mock- (dark blue) or UV- irradiated (light blue); EVs purified from infected cells (iEVs) and mock- (dark red) or UV-irradiated (light red); n=6 ±SEM shown. Two-way ANOVA performed, ** $p<0.01$, *** $p<0.001$. Tukey's post hoc test for iEV compared to control, EV, EV-UV, and iEV-UV $p=0.001$; for EV-UV and iEV-UV vs control and EV $p= 0.90$.

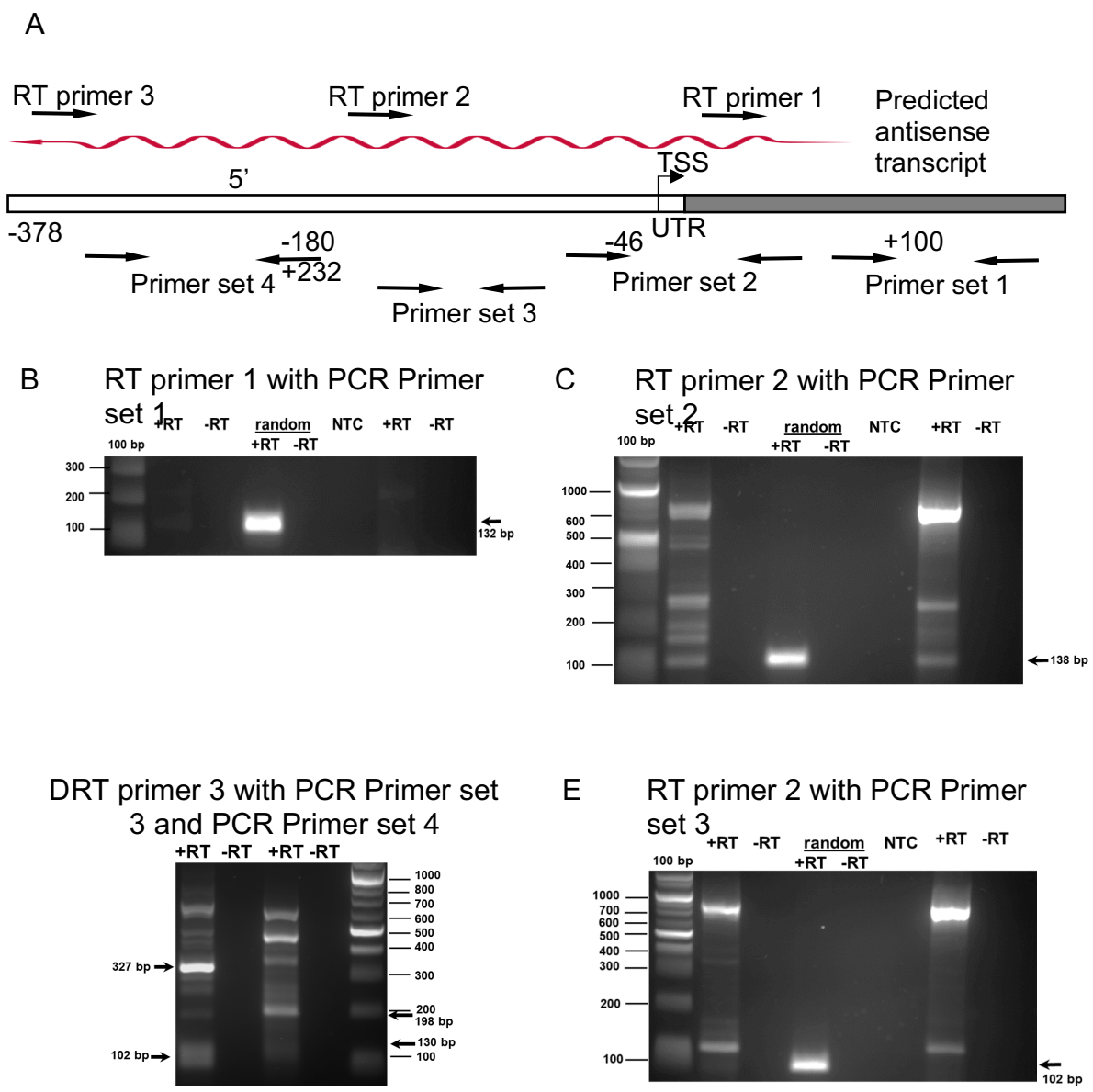

Supplemental Data Fig. 7. Genome scanning for an antisense lncRNA
A) Schematic representation of the stepwise walking upstream of the *DBH* gene to identify a putative antisense RNA (asRNA). The binding sites for the directional RT primers for asRNA detection are depicted. Primer sets 1-4 were used to amplify cDNAs produced by the directional primers as detailed below. The transcription start site (TSS), untranslated region (UTR) and protein coding region (grey) are highlighted. **B-E)** DBH antisense RNA detected in *T. gondii*-infected PC12 cells. Agarose gel resolution of PCR products from directional reverse transcriptase (RT) primers. Control reactions lacking reverse transcriptase (-RT) were performed for each sample. Random hexamer primers that will detect both + and – strands in reverse transcription reactions were also tested. **B)** asRNA was not detected as a PCR product (132 bp) using directional RT primer 1 (+13) and PCR primer set 1 (+100 to +232) although the random hexamer primers yielded a band indicating *DBH* mRNA. **C)** asRNA from directional RT primer 2 (-180) was detected by PCR primer set 2 (-46 to +92) as a PCR product

(138 bp). Additional bands are visible. **D)** Directional RT primer 3 (-378) detected asRNA with amplification by PCR primer set 3 (-153 to -51) with a PCR product (102 bp) and by PCR primer set 4 (-310 to -180) with 130 bp PCR product. Unexpected bands at 327 bp and 198 bp are due to amplification using the RT primer 3 and reverse primers for PCR primer set 3 and 4, respectively. **E)** First strand synthesis with RT primer 2 and PCR with primer set 3 yielded an unexpected band at 129 bp rather than the predicted 102 bp band. This was due to PCR amplification utilizing RT primer 2 and the reverse primer in set 3. PCR products of bands on gels were confirmed by DNA sequencing.

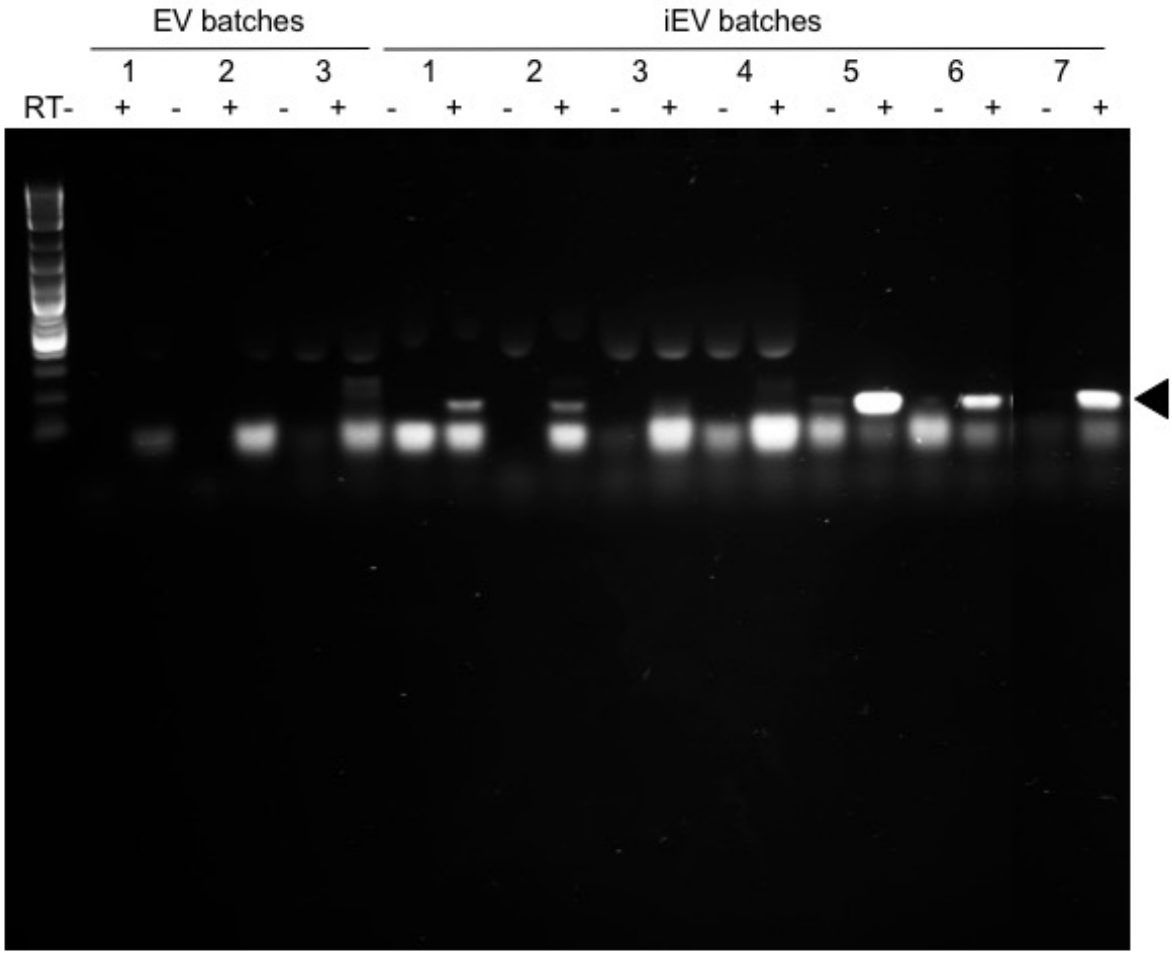

Fig. S7. Agarose gel image of EV lncRNA PCR products. The RT-PCR products resolved on a 1.5% agarose:TAE gel as in Fig 2D are shown for the full gel image. Products of EV RNA from uninfected PC12 cultures (n=3) and infected cultures (n=7) are shown with alternating lanes lacking reverse transcriptase. The PCR product (138 bp) is denoted by an arrowhead. The product was verified by cloning and sequencing. The first lane is a DNA ladder (NEB 1 kb plus). A lower spurious band appeared in some lanes .

SUPPLEMENTAL DATA TABLE

1: Primer sequences used throughout.

Name		Sequence
Rodent DBH	F	5’-CCACAATCCGGAATATA-3’
	R	5’-GATGCCTGCCTCATTG-3’
Human DBH	F	5’-GAAACGACTCCTCAGGCAT-3’
	R	5’-TCGCAGAGTAGAGTGCACA-3’
Rodent MAP2	F	F 5’-AAGGTGGTGGACGTGTG-3’
	R	5’-CTGGTTCATTGCCATTCTC-3’
Rodent GAPDH	F	5’-GTGGACCTCATGGCCTACAT-3’
	R	5’-TGTGAGGGAGATGCTCAGTG-3’
Human GAPDH	F	5’-AGGGCTGCTTTTAACTCTG-3’
	R	5’-CCCCACTTGATTTTGGAG-3’
Rat DBH MSRE	F	5’-CAGGACGTAGCCACAGATGG-3’
	R	5’-TGCCTTCCCCGGG-3’
Human DBH MSRE	F	5’-CAATACCCCAGAGGGGAGAG-3’
	R	5’-GCTTTCCCATCAGGACATGC-3’
Primer Set 1	F	5’-CCCACCGAACAGACATAA-3’
	R	5’-ACAGCAGTGCCATACAT-3’
Primer Set 2	F	5’-TCCTGGTCATCCTGGTG-3’
	R	5’-GGATGATCTCCTGGTCATAG-3’
Primer Set 3	F	5’-GAGGATCGGAGCAAAGT-3’
	R	5’-GCCAGGCTGTACCTAAT-3’
Primer Set 4	F	5’-TATGAGGCATTCAGCAG-3’
	R	5’-CATCATCAAGAGAATCGAAG-3’
RT-Primer 1 (lncRNA DBH)	F	5’-CCTCACCTCAGCCACCAG-3’
RT-Primer 2 (lncRNA DBH)	F	5’-TCCATGCGTCATTAGTGTCAA-3’
RT-Primer 3 (lncRNA DBH)	F	5’-CACTCACTGTCACTCAGGAAGG-3’